Revision 1

Word count: 8,368 (main text)

Evaluation of the Rietveld method for determining content and chemical composition of inorganic X-ray amorphous materials in soils

SILEOLA JOSEPH AKINBODUNSE[a], KRISTIAN UFER[b], REINER DOHRMANN[b,c], CHRISTIAN MIKUTTA[a,*]

[a]Soil Mineralogy, Institute of Mineralogy, Gottfried Wilhelm Leibniz University Hannover, Callinstr. 3, D-30167 Hannover, Germany

[b]Federal Institute for Geosciences and Natural Resources (BGR), Stilleweg 2, D-30655 Hannover, Germany

[c]State Authority of Mining, Energy and Geology (LBEG), Stilleweg 2, D-30655 Hannover, Germany

***Correspondence**

c.mikutta@mineralogie.uni-hannover.de

Keywords

Amorphous inorganic materials, soil, XRD, Rietveld analysis, mineralogical budgeting, quantification, chemical composition

ABSTRACT

Inorganic X-ray amorphous materials (iXAMs) such as vitreous phases, minerals having an insufficient number of repeating structural units to diffract X-rays, and inorganic solids with exclusively structural short-range order are ubiquitous in soils and relevant for numerous environmental processes, but are notoriously difficult to identify and quantify. To test for the quantification and chemical composition of iXAMs in soil, we prepared four mineral mixtures containing quartz, calcite, feldspars, and clay minerals in different proportions typical of soils and amended them with 10–70 wt% iXAMs in the form of a 1:1 weight mixture of ferrihydrite and opal-A. We quantified these iXAMs in mineral mixtures by analyzing powder X-ray diffraction (PXRD) data using the Rietveld method and compared the results for different sample preparation techniques (conventional and spray drying) based on the internal standard method in Rietveld analysis. The mineral mixtures were also analyzed for their chemical composition by X-ray fluorescence (XRF) spectrometry, and mass balance calculations combining Rietveld and XRF data were carried out to estimate the chemical composition of iXAMs in mineral mixtures. Both sample preparation methods showed no significant difference in determined iXAM contents and yielded accurate results for iXAM contents within ±3 wt% at the 95 % confidence level (2σ). The relative accuracy deteriorated with decreasing iXAM content, but remained below 10 % for iXAM contents > 10 wt% (mean = 3 %). The precision of iXAM content quantification in mineral mixtures prepared by spray drying was slightly better though statistically equivalent to the conventionally prepared mixtures (2σ = 1.49 and 1.61 wt%). The average precision of both sample preparation methods was ±2 wt% at the 95 % confidence level. Levels of detection and quantification of iXAMs in spray-dried mineral mixtures containing 1–10 wt% iXAMs were estimated at 0.8 and 4.0 wt%, respectively. The chemical composition of iXAMs in terms of major oxides was accurately assessed by mass balance calculations with average relative errors for nominal SiO_2 and Fe_2O_3 contents of 9.4 and 4.3 %, respectively (range = 0.02–54.7 %). Even though adsorbed H_2O and structural

H_2O/OH^- as quantified by the loss on ignition comprised an important portion of the iXAMs (15.3 wt%), their LOI in mineral mixtures as derived from mass balance calculations could only be quantified with an average relative error of 67.2 % (range = 1.30–371 %). We conclude that iXAMs in soil and related geomaterials present at levels > 4 wt% can be quantified by Rietveld analysis of PXRD data with an accuracy of ±3 wt% at best. Combined results of Rietveld and XRF analyses can yield accurate results for the chemical composition of iXAMs within a relative error of 10 % for major oxides, provided iXAM contents exceed 10 wt% and the content and chemical composition of all crystalline mineral phases is accurately assessed. The results presented in this study lay the foundation to explore iXAM contents and chemical compositions in soils and to examine their impact on soil physicochemical properties and biogeochemical element cycles.

INTRODUCTION

In condensed matter physics, material sciences, and chemistry the term 'amorphous' (from the Greek *a*, without, *morphé*, shape, form) refers to the absence of structural long-range order, that is, periodicity, in a substance. In contrast, the term 'X-ray amorphous', defines solids that do not exhibit sharp Bragg peaks in their X-ray diffraction (XRD) patterns, but are only detectable by broad diffuse X-ray scattering peaks. X-ray amorphous materials (XAMs) in soils are present as organic and inorganic compounds. The former materials, consisting of particulate and mineral-associated organic matter, are usually removed prior to XRD analysis using oxidants such as H_2O_2, NaOCl, and $Na_2S_2O_8$ (Jones et al. 2000; Mikutta et al. 2005a; Manaka 2006; Zabala et al. 2007). Therefore, XAMs recognizable in XRD patterns of soil samples by elevated background levels are predominantly inorganic in nature. Inorganic X-ray amorphous materials (iXAMs) in soil encompass a great variety of materials, such as vitreous phases, minerals having an insufficient number of repeating structural units to diffract X-rays, so-called 'short-range order', 'non-crystalline' or

'poorly crystalline' minerals, and inorganic solids with variable elemental composition and exclusively structural short-range order, often termed 'mineraloids'. Paracrystalline minerals like allophane, imogolite, ferrihydrite, and vernadite as well as amorphous silica, are typical examples (Higashi and Ikeda 1974; Taylor and Schwertmann 1974; Walker 1983; Parfitt and Childs 1988; Wada 1989; Kaufhold et al. 2010; Lessovaia et al. 2014, 2016; Casetou-Gustafson et al. 2018; Zahoransky et al. 2022). The quantities of iXAMs in soils vary a lot. They can range from 1 to 15 wt% in fine earth fractions (< 1 or < 2 mm) (Zabala et al. 2007; Tamppari et al. 2012; Lessovaia et al. 2014; Casetou-Gustafson et al. 2018), and generally increase with decreasing particle size (Manaka 2006). The highest iXAM contents of up to 47–77 wt% have been reported for clay fractions (< 2 μm) (Jones et al. 2000; Manaka 2006; Lessovaia et al. 2016).

Inorganic XAMs in soils play a crucial role in biogeochemical processes such as mineral weathering, carbon sequestration, and sorption reactions of nutrients and pollutants (Hellmann et al. 1990; Filgueiras et al. 2002; Abollino et al. 2011; Ruiz-Agudo et al. 2012, 2016; Basile-Doelsch et al. 2015; Bazilevskaya et al. 2018). They also exert great influence on soil physical properties such as aggregate stability, permeability, cementation, friability, porosity, surface area, bulk density, clay dispersion, and hydraulic conductivity (Goldberg 1989; Jones et al. 2000; Sanborn et al. 2011; Rawlins et al. 2013; Lehtinen et al. 2014; Totsche et al. 2018). Therefore, accurate and fast methods for quantitative analysis of iXAMs in soils and their parent materials are of great importance. Wet-chemical extractions have become the standard in soil science for selective removal of iXAMs from soils. The most commonly employed extractants are acid ammonium oxalate, ascorbic acid, disodium 4,5-dihydroxy-1,3-benzenedisulfonate (Tiron), ethylenediaminetetraacetic acid (EDTA), and hydroxylamine (NH_2OH) (Rennert 2019, Rennert et al. 2021). The main drawback of wet-chemical extractions to quantify the total iXAMs content in soil is their element selectivity and ability to even dissolve crystalline materials (Schwertmann and Taylor 1972; Higashi and Ikeda 1974; Taylor and Schwertmann 1974; Walker 1983; Parfitt and Childs 1988; Wada 1989; Dohrmann et al. 2002; Kaufhold et al. 2010). In contrast, powder X-ray

diffraction (PXRD) in combination with extraction methods offers much greater potential for iX-AMs quantification in soils than chemical extractions alone. In fact, PXRD has long been used to study amorphous solids in soils (Brydon and Shimoda 1972; Ross 1980; Schwertmann et al. 1982; Blank and Fosberg 1991). In its simplest application, PXRD is used to identify XAMs by the appearance of 'amorphous humps' in X-ray diffractograms (DeMumbrum 1960; Blank and Fosberg 1991). In more sophisticated applications, PXRD are recorded before and after treatment of soil solids with selective extractants used to dissolve specific amorphous components (Schwertmann et al. 1982; Kodama and Wang 1989). Far fewer studies utilized quantitative phase analysis (QPA) of PXRD data, which relies on the fact that the abundance of a crystalline phase relates to the intensity of its X-ray diffraction peaks. Among QPA methods, the Reference Intensity Ratio (RIR) method, also known as the matrix flushing method after Chung (1974), has been most popular in past decades. The method involves comparing the intensity of one or more peaks of a phase with the intensity of a peak of an internal standard (usually the 113 reflection of corundum) in a 50:50 wt% mixture. Once the RIR values for all crystalline phases in a sample are known, the weight abundance can be determined for every crystalline phase in the sample. The content of XAMs can then be calculated by difference to 100 wt%. The RIR method may suffer from effects of variable chemistry and preferred crystal orientation, since only one or a series of reflections are used.

A second method for QPA of PXRD data involves fitting of XRD standard patterns to an entire sample pattern to obtain quantitative abundances of both crystalline and X-ray amorphous components ('full profile fitting method', FULLPAT) (Chipera and Bish 2002, 2013). This method is similar to the RIR method, but utilizes the entire diffraction pattern rather than single reflections, including the background signal that contains information of sample composition and matrix effects. Here, amorphous or disordered materials are accounted for by their individual XRD patterns (standard patterns). Full profile fitting thus allows the direct quantification of XAMs without the addition of an internal standard and has proven successful in QPA of unknown samples (Omotoso et al. 2006; Casetou-Gustafson et al. 2018). Similar to the RIR method, this type of QPA re-

quires that phases used as standards do not significantly differ from the respective phases in the sample in terms of chemical composition and structure and that standards and samples are measured with the same instrument settings.

The third popular method of QPA of PXRD data is the Rietveld method, which involves constructing a model consisting of crystal structures of all component phases (Rietveld 1969; Bish and Post 1993). In Rietveld refinements, differences between observed and simulated diffraction patterns are minimized by varying model parameters, including scale factors related to phase abundances, unit-cell parameters, and crystallite size and strain-broadening parameters for each phase. Atomic positions and site occupancies can be varied as well (Rietveld 1969). The method provides information on all phases with long-range order (crystalline phases), while XAMs are quantified as one entity. Usually, the Rietveld method normalizes the summed mass fractions of crystalline components to unity. Determining the amorphous fraction in a sample involves blending the sample with a known amount of an internal standard (e.g., corundum). If amorphous material is present, the Rietveld-determined mass fraction of this standard is higher than the amount mixed with the sample. The mass fraction of XAMs is then calculated as:

$$\text{XAMs} = (S_R - S) / [S_R (1 - S)], \quad (1)$$

where S is the mass fraction of the standard and S_R is the Rietveld-determined standard mass fraction. Once the mass fraction of XAMs is determined, the final mass fraction of a crystalline component X_i is calculated from a Rietveld refinement of the non-spiked sample according to:

$$X_i = (1 - \text{XAMs}) \times X_{iR}, \quad (2)$$

with X_{iR} being the Rietveld-determined mass fraction of phase X_i (Jones et al. 2000).

Although the Rietveld method has some advantages over the conventional quantitative XRD approach (RIR method) in terms of accuracy and detection limits (Rietveld 1969; Bish and Post 1993; Gualtieri 2000; Chipera and Bish 2002), it also suffers from limitations such as missing or

inappropriate structure models and inadequate sample preparation. The first point is of particular importance because clay minerals in soils are often disordered. Over the past 15 years, Ufer and coworkers developed disorder models for full-pattern Rietveld refinement of PXRD data of expandable clay minerals of the smectite group (Ufer et al. 2004; Szczerba and Ufer 2018; Wang et al. 2018) and later of interstratified expandable clay minerals such as illite-smectite (Ufer et al. 2012a). Recently, first models were developed for hydroxy-interlayered minerals (HIMs) present in acidic soils (Dietel et al. 2019a, 2019b). Provided appropriate structure models are available, sub-optimal sample preparation for PXRD analysis can also spoil the outcome of Rietveld refinements. Conventional sample preparation often leads to preferred orientation, which occurs when the crystallites in a powder are not randomly oriented, that is, when there is a greater probability for the crystallites to be oriented in one particular direction than in the others. The effect of preferred orientation, which is most pronounced for phyllosilicate minerals, can be corrected to some extent in Rietveld refinements by mathematical functions such as the March function or spherical harmonics (Dollase 1986; Ahtee et al. 1989; Järvinen 1993; Gualtieri 2000). However, the best way to counteract preferred orientation is to avoid it. For this, spray drying of powdered samples has been proven to be very effective for QPA (Smith et al. 1978; Hillier 1999a).

Despite advanced knowledge on the application of quantitative PXRD to geomaterials, information on Rietveld-determined quantities of iXAMs in soils is limited (Weidler et al. 1998; Jones et al. 2000; Manaka 2006; Zabala et al. 2007; Tamppari et al. 2012; Lessovaia et al. 2014, 2016; Casetou-Gustafson et al. 2018). Perhaps the most obvious reason for this is the complex sample matrix, which can contain highly disordered clay minerals, solid solutions, and structurally well-defined minerals with distinct crystal defects. These factors may limit the success of Rietveld analysis for iXAM quantification in soils. Poor accuracy and/or reproducibility of iXAM contents determined by Rietveld analysis inevitably leads to high uncertainty in the chemical composition of iXAMs. The chemical composition of iXAMs can be estimated from mass balance calculations using the Rietveld-based iXAM content and information on chemical sample composition as ob-

tained by, for example, X-ray fluorescence (XRF) spectrometry ('balance sheet method' or 'mineral budgeting approach') (Jones et al. 2000; Andrist-Rangel et al. 2006). To this end, XRF-based oxide contents and loss on ignition (LOI) are first assigned to each crystalline phase, usually by assuming ideal stoichiometry, and the non-explained oxide fractions and LOI are then assigned to XAMs (Jones et al. 2000; Cesarano et al. 2018).

To date, we are lacking information on the basic performance of the Rietveld method for iXAM quantification in soils. Data on analytical method characteristics such as accuracy, precision, and limits of detection and quantification are not currently available. Because of this lack of knowledge, it is currently impossible to reliably assess abundance and chemical composition of iXAMs in soils, establish quantitative relationships with physicochemical soil properties, and evaluate iXAM fractions dissolved by routinely applied wet-chemical soil extractions. Thus, our main objectives were (1) to evaluate the accuracy and precision of iXAM quantification using Rietveld analysis of PXRD data, (2) to determine Rietveld-based detection and quantification limits for iXAMs in soils or related geomaterials, (3) to test for the optimal way of PXRD sample preparation for iXAM quantification, and (4) to examine the accuracy of chemical iXAM analysis by mass balance calculations using Rietveld and XRF data ('balance sheet method'). To achieve these goals, we prepared mineral mixtures of increasing complexity, consisting of quartz, feldspars, carbonate, and clay minerals averaging the mineralogical composition of several European soils. We amended these mixtures with known amounts of synthetic iXAMs and analyzed their content and chemical composition by Rietveld refinements of PXRD data and XRF spectrometry. For PXRD measurements, the mixtures were either spray-dried or directly loaded into XRD sample holders ('conventional sample preparation'). The obtained information serves as a framework for future Rietveld-based PXRD studies on iXAMs in soils or related geomaterials that address their ecological relevance.

MATERIALS AND METHODS

Samples and sample preparation

Minerals of this study were obtained from the mineral collection of the Federal Institute for Geosciences and Natural Resources (BGR), Hannover, Germany. Table 1 summarizes information on their origin, nominal formulas, and purity. Five to seven minerals were mixed in different mass ratios (Table 2) to approximate the average mineral composition of European Luvisols developed on loess (w/o carbonate) (Tarrah et al. 2000; Pospíšilová et al. 2021), Cambisols or Podzols developed on granite (Gudmundsson and Stahr 1981; Žigová et al. 2013), and a marly glacial till (Scheffer and Schachtschabel 2010). Before blending minerals together, each mineral was ground to a particle size < 5 μm (~ 4 mL mineral plus 10 mL ultrapure water; resistivity: ≥ 18.2 MΩ cm) for 5–10 min with a McCrone micronizing mill using cylindrical ZrO_2 grinding elements. The minerals were then oven-dried at 60 °C. One part of the mineral mixtures was spiked with an internal standard (30 wt% corundum) to determine their inherent amorphicity and the amorphicity induced by grinding and mixing. The other part was blended with different proportions of synthetic iXAMs (10–70 wt%) consisting of ferrihydrite and opal-A in a 1:1 mixture by weight, and then spiked with an internal standard before proceeding with PXRD analysis. Ferrihydrite and opal-A were used because they are important soil iXAMs, which can constitute > 10 wt% of soil clay fractions (Mikutta et al. 2005b; Lessovaia et al. 2016). As an internal standard, we used corundum Baikalox CR1, a high-grade, crystalline reference material with a particle size of < 2 μm. The low amorphicity potentially associated with the corundum was insignificant when compared to the amount of amorphous material in the mineral mixtures.

Tables 1 and 2

Appropriate amounts of internal standard blended with samples are crucial for Rietveld-based quantification of XAMs, since the amorphous fraction is calculated from the Rietveld-determined mass fraction of the standard. Various spike levels have been used in the past. Hillier (2000) used

10 wt% for an artificial sandstone mixture containing 19.8 wt% glass, while Ufer et al. (2008) utilized a spike of either 10 or 20 wt% for smectite-rich bentonites. According to Jones et al. (2000), a smaller spike (10 wt%) is a good choice for samples with high amorphous content and a higher spike level (50 wt%) is better suited for samples with low amorphous contents, while a spike level of 30 wt% was considered a good compromise for soils with amorphous content of 28–77%. This is due to the need to find a compromise between the best possible sensitivity and over-dilution of the sample by the standard (Jones et al. 2000; Westphal et al. 2009). Therefore, we also used a spike level of 30 wt% to obtain an adequate signal from the standard for the different iX-AM concentrations in the mineral mixtures.

For conventional PXRD sample preparation, minerals were mixed in an agate mortar with ethanol as grinding aid. Another portion of mineral mixtures was spray-dried following Hillier (1999a) to minimize the effect of preferred orientation on QPA results. For this, we employed the rocket-shaped spray dryer manufactured by the James Hutton Institute (Aberdeen, Scotland, UK). Before spray drying, mineral powders were mixed with ultrapure water containing 0.5 wt% poly-vinyl alcohol ($[\text{-}CH_2CH(OH)\text{-}]_n$, molecular weight: ~ 22 kDa, VWR) and 0.1 wt% of 1-octanol ($CH_3(CH_2)_7OH$, Thermo Fisher Scientific). The solid-to-liquid ratio (w/v) ranged from 1:3 to 1:5. Polyvinyl alcohol helped to bind the dried product, while 1-octanol prevented foaming during so-lution dispersion and formation of air bubbles in the dried granules, and facilitated the transfer of samples between containers (Hillier 1999a). Afterwards, the slurries were homogenized for 60 s in a McCrone mill. The spraying pressure was around 69 kPa (10 psi) and the temperature of the inner chamber was set at 155 °C. Dried granules were collected on a sheet of wax paper placed at the bottom of the drying cylinder. Product recovery was around 60–65 % for sprayed samples. The spray-dried mineral mixtures were composed of round-shaped aggregates with rough surface textures and sizes ranging from 40 to 100 μm (Fig. 1).

Figure 1

252 **X-ray diffraction and Rietveld analysis**

253 X-ray diffraction patterns were recorded on a Bruker D8 diffractometer in Bragg-Brentano
254 geometry (θ-θ goniometer) using CuKα radiation generated at 40 kV and 40 mA. The instrument
255 was operated with a 0.2 mm divergence slit, 2.5 º primary and secondary Soller slits, a 2.459 º
256 detector opening, and a high-resolution Lynxeye XE-T detector. Samples were measured from 3 to
257 100 º2θ with a step size of 0.006 º2θ and a measuring time of 1.8 s per step. Mineral mixtures pre-
258 pared conventionally were measured with rotation (30 rpm), while spray-dried mixtures were
259 measured without rotation because of the flowability of the powder. The top-loading technique
260 was used for sample transfer into 25-mm plastic sample holders.

261 Rietveld refinements of PXRD data were performed in BGMN with Profex v.5.0.1 as graph-
262 ical user interface (Döbelin and Kleeberg 2015). Profex-BGMN uses information on instrumental
263 features such as primary beam, secondary beam (mode and length of divergence slit, opening an-
264 gle of Soller slits, axial beam mask, and sample stage), wavelength distribution of the X-ray
265 source, instrument detector, and the contribution of phases such as crystallite size and micro strain
266 for the configuration of peak profiles. The peak shape function can be described by the deconvolu-
267 tion of wavelength distribution, instrument function, and sample function (crystallite sizes and
268 micro strain broadening). Prior to Rietveld refinement, simulation by the Monte Carlo ray-tracing
269 algorithm was used to obtain instrument profile functions, and instrumental profile shapes were
270 calculated at different angular steps (Bergmann et al. 1997, 1998; Döbelin and Kleeberg 2015).
271 Instrument parameters were set and remained unchanged during Rietveld analyses, while sample
272 functions were refined. The degree of polynomial was defined for background refinement (RU =
273 10 or 11) and the upper and lower limits were defined (if necessary) for each parameter present in
274 a structure model. These parameter limits were either fixed as predefined in structure models or
275 modified to improve the stability of refinement and the convergence of refined parameters. Statis-
276 tical parameters (R_{wp}, R_{exp}, and 'goodness of fit', GOF) were used to evaluate the quality of re-
277 finements. GOF equals R_{wp} divided by R_{exp}, where R_{wp} represents the weighted residual square

sum assessing the difference between measured and calculated diffractograms, while R_{exp} is the lowest obtainable value of R_{wp} (Döbelin and Kleeberg 2015).

Profex-BGMN is well suited for our samples because it is able to handle structure models for stacking disordered clay minerals such as illite-smectite and kaolinite, or turbostratically disordered smectite (Ufer et al. 2004, 2008, 2012b, 2015). Turbostratic disorder of interlayered materials, described as a 'random rotation and/or translation of individual layers relative to each other' (Ufer et al. 2004, 2008), yields irregular asymmetric non-basal reflections and peak shapes which cause problems during refinement with standard models and thus QPA if not adequately accounted for. In addition, the mass fractions of amorphous and individual crystalline components can be directly estimated with Profex-BGMN if the mass fraction of an internal standard is fixed before starting the refinement. We generally used structural input models of ordered phases provided in the Profex-BGMN structure file library. Disordered structure models for illite-smectite, kaolinite, and smectite were taken from the literature (Ufer et al. 2008, 2012b, 2015). Powder XRD patterns were refined between 5 and 80 °2θ. By applying the predefined upper and lower limits of parameters as given in structure models, we refined lattice constants, phase fractions, preferred orientation by applying symmetrized harmonics (Bergmann et al. 2001) of the orders zero to six, micro strain, and isotropic line broadening, while the zero point, sample displacement, and background of powder patterns were refined as non-structural parameters. Occupation factors of cations in models remained unchanged during refinements. Refinement of preferred orientation was ignored for all spray-dried samples (order set at zero) to reveal the effect of spray drying on preferred orientation. Similarly, mineral phases present in trace amounts (< 1 wt%) in illite-smectite, kaolinite, and smectite-rich bentonite (Table 1) were ignored during Rietveld analysis of mineral mixtures.

301 **Scanning electron microscopy**

302 For the determination of particle size and morphology of mineral mixtures, samples were dis-
303 persed on an adhesive carbon disc, sputtered with Au, and analyzed by a JEOL JSM-7610FPlus
304 field emission scanning electron microscope to obtain secondary electron images. The probe cur-
305 rent was set between 10 and 20 pA at an accelerating voltage of 5 kV, and the working distance
306 ranged from 2 to 3 mm.

307

308 **X-ray fluorescence spectrometry**

309 The chemical composition of mineral mixtures was analyzed by wavelength-dispersive XRF
310 spectrometry using a PANalytical Zetium spectrometer. Approximately one gram of oven-dried
311 (105 °C) mineral mixtures was weighed to the 4^{th} decimal place, then heated at 1030 °C for
312 10 min, cooled in a desiccator, and reweighed to determine the LOI. Elements or compounds lost
313 during heating include organics, CO_2, SO_2, Cl, and structural water. The remaining ignited sam-
314 ples were mixed with 5.0 g lithium metaborate (Spectroflux 100A, Alfa Aesar) and 25 mg of lithi-
315 um bromide and fused at 1200 °C for 20 min in a Herzog HAG 12/1500 fusion digestion unit. The
316 obtained glass disks were analyzed by XRF spectrometry. Instrument calibrations were validated
317 by analysis of reference materials, and in-house standards as well as 130 certified reference mate-
318 rials were used for data correction procedures.

319

320 **Thermogravimetry and calorimetry analyses**

321 Ferrihydrite, opal-A, and their 1:1 mixture were analyzed by thermogravimetry (TG) and dif-
322 ferential scanning calorimetry (DSC). TG-DSC measurements were carried out using a Setsys
323 Evolution 1750 instrument (SETARAM). Samples were heated from 25 to 1000 °C at a rate of
324 5 °C/min under a flow of N_2 set at 30 mL/min.

325

Data analysis

Statistical analyses were performed in SigmaPlot v.15 (Inpixon GmbH). Data were evaluated by test statistics and linear regression analyses. Significant differences between variable groups were evaluated by Student's and Welch's t-tests, Mann-Whitney rank sum test, and one-way analysis of variance (ANOVA) with subsequent post-hoc tests for multiple comparisons (Holm-Sidak method and Tukey test). Normality of data and homogeneity of variances were analyzed using the Shapiro-Wilk and Brown-Forsythe test, respectively. Differences were considered significant at $p < 0.05$. The accuracy ('true value') of iXAM content and composition was evaluated by comparing nominal and Rietveld-based values, while the precision of iXAM quantification was determined by repeated (N = 5) sample preparation (mixing of mineral mixture with 10 wt% iXAMs and 30 wt% corundum, followed by convention sample preparation and spray drying) and Rietveld analysis of selected mineral mixtures. Detection and quantification limits of iXAMs were evaluated following DIN 32645 as described in Funk et al. (2005). The quantification limit was calculated with a maximum admissible error of the analytical result of 10 % (*k*-value).

RESULTS

In the following, we first detail aspects of sample preparation and general Rietveld fit quality. We then address accuracy, precision, and limits of detection and quantification of the Rietveld method for iXAM quantification. Afterwards, we examine the accuracy of the Rietveld method for crystalline mineral components in mineral mixtures before applying the balance sheet method to quantify the chemical composition of iXAMs in mineral mixtures and evaluating the accuracy of this approach.

Sample preparation and Rietveld fit quality

Figure 2 displays diffractograms of conventionally prepared ferrihydrite and opal-A, and their 1:1 mixture prepared conventionally and by spray drying. Apparently, spray drying of iXAMs at 155 °C did not alter their diffractogram, documenting the absence of iXAM transformations into more crystalline phases during spray drying. Spray drying also effectively eliminated the effect of preferred orientation for clay minerals. Figure 3 compares diffractograms of mineral mixtures C and D prepared conventionally and by spray drying. Mixture C represented the least complex mineral mixture, while mixture D was the most complex, as it contained the highest numbers of minerals and disordered clay minerals. For chlorite in both mixtures, 00*l* reflections at 6.17, 12.4, 18.6, and 24.9 °2θ, when scaled to the quartz 1-10 reflection at 20.8 °2θ, were strongly reduced after spray drying. Similarly, the broad peak of the disordered illite-smectite at 7.5–9.2 °2θ was markedly reduced in the spray-dried mixtures (Fig. 3).

Figures 2 and 3

Figure 4 shows an example of Rietveld fits for mineral mixture B containing 40 wt% iXAMs and both sample preparation methods. The figure illustrates that peak intensities were correctly matched in both cases. Generally, significantly smaller GOF values ($p < 0.001$) were recorded for conventionally prepared mixtures (Tables S1 and S2). For all analyzed mineral mixtures with or without iXAMs that were conventionally prepared, GOF values ranged from 1.23 to 1.84 (mean = 1.44), while GOF values for spray-dried mixtures ranged from 1.44 to 1.90 (mean = 1.63). Likewise, for individual mineral mixtures A–D with 0–70 wt% iXAMs, the conventional sample preparation always resulted in significantly lower GOF values ($p \leq 0.028$) than spray drying (Table S2). We found that the addition of iXAMs to mineral mixtures resulted in lower GOF values compared to the original mineral mixtures, and slightly higher GOF values at the upper end (> 50 wt%) of nominal iXAM contents for all mineral mixtures and sample preparation methods (Table S1). The reason for the higher GOF values for the spray-dried compared to the conventionally

prepared mineral mixtures is that correction for preferred orientation by spherical harmonics was not applied during Rietveld refinements, and thus fewer parameters were refined. Comparisons of GOF values for different mineral mixtures revealed that sample composition had a significant effect on Rietveld fit quality only for the conventionally prepared mixtures, caused by mixture B (Table S2).

Figure 4

Quantification of iXAMs

We tested the accuracy of iXAM quantification in mineral mixtures depending on the complexity of crystalline mineral assemblages for both sample preparation methods. The abundances of iXAMs in mineral mixtures determined by the Rietveld method are illustrated in Figure 5, and Table 3 summarizes values of iXAM contents along with estimated standard deviations as well as absolute and relative quantification errors. Linear relationships between nominal and Rietveld-derived iXAM contents with R^2 values > 0.99 and regression slopes of 0.94–0.98 for the conventionally prepared mixtures and of 0.95–0.99 for the spray-dried mixtures (Fig. 5) confirm a high degree of accuracy in iXAM quantification for both sample preparation methods and different mineral assemblages. We found no significant difference between regression slopes for both sample preparation methods ($p = 0.855$). QPA results obtained by Rietveld refinements indicated that all starting mineral mixtures with 0 wt% nominal iXAM contents contained an intrinsic amount of amorphous materials and amorphicity induced during sample preparation by milling and mixing of 1.18–3.92 wt% (Fig. 5, Table S1). This intrinsic amorphous part also includes phases that are contained in trace amounts (i.e., not quantifiable by Rietveld) and the amorphous portion of crystalline phases.

Figure 6 illustrates the frequency distribution of the deviation between nominal and Rietveld-determined iXAM contents in all mineral mixtures for both sample preparation methods after correction for the intrinsic and milling/mixing induced amorphicity of crystalline phases. This data

399 shows that absolute errors of iXAM determination were within ±2 wt% for both sample prepara-
400 tion methods with no gross outliers. The error distributions were non-Gaussian and suggested a
401 slight tendency of iXAM overestimation, which was less pronounced for the spray-dried mineral
402 mixtures. Nonetheless, neither method led to a significant difference in absolute quantification
403 errors (Mann-Whitney rank sum test, $p = 0.922$, $N = 28$). Relative errors of Rietveld-determined
404 iXAM contents ranged from 0.31 to 13.3 % and increased with decreasing iXAM content (Fig. 7).
405 Conventionally prepared mineral mixtures resulted in a larger spread of relative errors for nominal
406 iXAM contents < 50 wt% when compared to the spray-dried mineral mixtures (Fig. 7). Means and
407 standard deviations (2σ, equivalent to the 95 % confidence level) of iXAM quantification errors
408 for each mineral mixture are listed in Table 4. Statistical tests for individual mineral mixtures (A–
409 D) showed that there were no significant differences in absolute iXAM quantification errors be-
410 tween both sample preparation methods. Combined means ± 2σ of absolute quantification errors
411 for the four mineral mixtures were 0.14 ± 2.47 and 0.16 ± 2.21 wt% for the conventional and
412 spray drying sample preparation method, respectively. Consequently, absolute errors in iXAM
413 quantification appear to be indifferent for both sample preparation methods. The total absolute
414 quantification error (mean ± 2σ) calculated from all mineral mixtures and sample preparation
415 methods was 0.15 ± 2.32 wt% ($N = 56$).

416 **Figures 5-7, Tables 3 and 4**

417 Figure 8 shows the results of iXAM quantification based on repetitive sample preparation and
418 analysis ($N = 5$) of mineral mixtures B–D amended with 10 wt% iXAMs. Absolute errors in iX-
419 AMs quantification ranged from -1.69 to 1.11 wt% for the conventionally prepared mixtures
420 (mean ± 2σ = -0.21 ± 1.61 wt%) and from -1.08 to 1.24 wt% for the spray-dried mixtures (mean ±
421 2σ = 0.16 ± 1.49 wt%). These numbers imply that the spray drying resulted in more precise iXAM
422 results when compared to the conventional sample preparation method. However, we found no
423 significant effect of sample preparation method on average quantification errors of same mineral

mixtures (Fig. 8). We also found that mineral assemblage complexity only produced significant differences in iXAM quantification errors for the spray-dried mixtures (Fig. 8). Figure 8 also shows that mineral mixture D having the highest complexity produced the largest deviations from nominal iXAM contents for the spray-dried mixtures. Combining all data of Figure 8, the average precision of iXAM quantification ± 2σ was -0.03 ± 1.57 wt% (N = 30).

Figure 8

In order to determine limits of iXAM detection and quantification following DIN 32645, we amended mineral mixture B with 1–10 wt% iXAMs in ten concentration steps (Fig. 9). A regression slope of 1.00(2) and data points falling into the 95 % prediction band testify that iXAMs can be accurately determined by the Rietveld method. From the linear calibration function of nominal against Rietveld-derived iXAM contents – corrected for the amorphicity of the initial mineral mixture as constant factor – we obtained iXAM detection and quantification limits of 0.8 and 4.0 wt%, respectively. Absolute and relative method standard deviations were calculated to be 0.18 wt% and 3.26 %, respectively.

Figure 9

Chemical composition of iXAMs

For the accurate assessment of the chemical composition of iXAMs by the balancing of oxide masses obtained from PXRD and XRF data, the correct quantification of crystalline minerals in a given sample by the Rietveld method is a key prerequisite. Nominal vs. Rietveld-determined contents of crystalline minerals are exemplarily shown in Figures 10 and 11 for mineral mixtures C (lowest complexity) and D (highest complexity), respectively. Figures S1 and S2 show analogous data for mineral mixtures A and B, and Tables S1 and S3 summarize quantified mineral contents for all mineral mixtures and their errors. Generally, both sample preparation methods produced statistically similar absolute quantification errors for all crystalline minerals (quartz, feld-

spars, calcite, illite-smectite, chlorite, kaolinite, and smectite). The spray drying method occasionally proved to be more accurate in the quantification of feldspars than the conventional sample preparation method (Table S3). In general, however, we found no significant differences in feldspar quantification errors between mineral mixtures using either sample preparation method (Table S4). Both sample preparation methods resulted in an overestimation of disordered illite-smectite, with a tendency towards greater errors in spray-dried compared to conventionally prepared mineral mixtures (Figs. 11, S1, and S2).

Figure 12 shows histograms of quantification errors for all crystalline minerals and both sample preparation methods. As opposed to absolute quantification errors of iXAMs (Fig. 6), absolute quantification errors of crystalline minerals were normally distributed. Absolute quantification errors varied from -6.1 to 4.3 wt% for the conventionally prepared mineral mixtures (mean ± 2σ = -0.25 ± 2.94 wt%, N = 192) and from -3.8 to 4.1 wt% (mean ± 2σ = -0.31 ± 2.78 wt%, N = 192) for the spray-dried mixtures. The total mass bias of crystalline minerals determined for all iXAM levels ranged from 3.6 wt% in mixture C to 12.7 wt% (mean ± 2σ = 6.67 ± 4.96 wt%) in mixture A for the conventional sample preparation and from 2.5 wt% in mixture C to 12.2 wt% in mixture D for the spray-dried samples (mean ± 2σ = 6.62 ± 4.68 wt%). Generally, this indicates that there was only a small difference in the quantification of crystalline minerals between both sample preparation methods and that the total mass bias increased with increasing sample complexity.

Because the quantification of clay minerals is critical to arrive at an accurate chemical composition of soil iXAMs, we analyzed their Rietveld quantification errors in detail (Tables S5–7). For the sum of clay minerals (chlorite, illite-smectite, kaolinite, and smectite), we found no significant effects of sample preparation method and sample composition on their absolute quantification errors (Table S5). However, the complexity of mineral assemblages significantly affected Rietveld quantification errors for chlorite and illite-smectite (but not kaolinite), irrespective of sample preparation method (Table S6). Even though Rietveld quantification errors of illite-

473 smectite and kaolinite (but not chlorite) occasionally depended on the sample preparation method
474 for individual mineral mixtures, we generally found no significant effect of sample preparation
475 method on the quantification of individual clay minerals after pooling their data for all mineral
476 mixtures analyzed (Table S7).

477 **Figures 10-12**

478 Figure 13 illustrates the comparison between XRF- and Rietveld-derived oxide contents for
479 all initial mineral mixtures A–D and both sample preparation methods. The chemical composi-
480 tions of crystalline minerals were taken from structure models used in the Rietveld refinements.
481 XRF-derived chemical compositions of all initial mineral mixtures A–D and iXAM-amended
482 mineral mixtures B–D are summarized in Tables S8 and S9, respectively. For all initial mineral
483 mixtures and both sample preparation methods, SiO_2 and Fe_2O_3 contents derived from XRF spec-
484 trometry and Rietveld analysis always showed a good correspondence (±3 wt%) (Fig.13, Table
485 S8). There was also a good agreement (±2 wt%) between Al_2O_3, Na_2O, K_2O, CaO, and MgO con-
486 tents. XRF spectrometry results (Tables S8 and S9) showed that TiO_2 ($\geq$ 0.1 wt%.) was present in
487 mineral mixtures A, B, and D because of trace amounts of anatase in kaolinite, which remained
488 undetected by PXRD. The highest amount of TiO_2 was therefore recorded for mixture D having
489 the highest kaolinite content (Table 2). Generally, deviations between oxide contents determined
490 by XRF spectrometry and Rietveld analysis became more apparent for oxide concentrations < 4
491 wt% (Fig. 13).

492 Based on XRF and Rietveld data, we employed the balance sheet method to calculate the
493 chemical composition of iXAMs in mineral mixtures prepared conventionally and by spray drying
494 (Table S10). A detailed breakdown of the oxide mass balance calculation is exemplarily given in
495 Table 5 for the spray-dried mixture B containing 40 wt% iXAMs. Data in Table 5 illustrate that
496 the balance sheet method yielded an accurate iXAM chemical composition in terms of nominal
497 SiO_2 and Fe_2O_3 contents (absolute errors < 1.4 wt%), but a larger discrepancy between nominal

498 and XRF/Rietveld derived LOI of iXAMs (absolute and relative error = 1.39 wt% and 23 %, re-
499 spectively). The total oxide plus LOI content of 43.1 wt% determined by the balance sheet method
500 for iXAMs in this sample was identical within error to the iXAM content quantified by Rietveld
501 analysis (43.3 wt%; Table 5). The mass balance approach also resulted in the assignment of other
502 oxides than SiO_2 and Fe_2O_3 (e.g., Al_2O_3, Na_2O, and CaO) to the iXAM fraction of all analyzed
503 mixtures (Tables 5 and S10). However, their summed quantities generally remained below 3 wt%
504 (Table S11).

505 Figure 14 displays the mass-balance derived chemical composition of iXAMs in terms of
506 SiO_2, Fe_2O_3, and LOI contents as major constituents of the iXAMs used along with their relative
507 errors for mineral mixtures B–D and both sample preparation methods. In terms of SiO_2, Fe_2O_3,
508 and LOI contents, both sample preparation methods resulted in largely equivalent results (Table
509 S10). For all samples analyzed, deviations of quantified oxide contents from their nominal values
510 ranged from -2.64 to 1.51 wt% for SiO_2 (mean ± 2σ = 0.01 ± 2.39 wt%) and from -1.53 to 0.39
511 wt% for Fe_2O_3 (mean ± 2σ = -0.40 ± 0.96 wt%) (Table S12). Relative errors associated with these
512 numbers were 0.07–54.7 % for SiO_2 (mean ± 2σ = 9.39 ± 23.4 %) and 0.02–35.6 % for Fe_2O_3
513 (mean ± 2σ = 4.26 ± 12.20 %). The relative errors of the major two oxides were mostly within an
514 acceptable error limit of ±10 %, but can be much higher in complex mineral mixtures, especially
515 at low iXAM contents (Fig. 14).

516 The LOI comprising mainly adsorbed H_2O and structural H_2O/OH^- was an important constit-
517 uent of the iXAMs used in this study. XRF analysis of the 1:1 ferrihydrite-opal mixture delivered
518 a LOI of 15.3 wt%, which is close to the 14.0 % weight loss of the mixture upon heating up to
519 1000 °C during TG analysis (Fig. S3). The LOI determined for iXAMs in all mineral mixtures
520 deviated between 0.14 and 5.69 wt% from nominal values (mean ± 2σ = 2.19 ± 2.78 wt%), and
521 relative errors ranged from 1.30 to 371 % (mean ± 2σ = 67.2 ± 171 %) (Fig. 14). Pooling all sam-
522 ples for each sample preparation method, we obtained excellent linear relationships with an R^2 >

0.99 between the nominal and mass-balanced derived sum of SiO_2, Fe_2O_3, and LOI contents of iXAMs in the mineral mixtures (Fig. 15). Regression slopes were indifferent for both sample preparation methods and slightly lower than unity. The latter was caused by an overestimation of the LOI for iXAMs, particularly at the lower end of iXAM contents (Fig. 14, Table S12). There was no significant difference in absolute quantification errors of summed SiO_2, Fe_2O_3, and LOI contents between both sample preparation methods.

Figures 13-15, Table 5

DISCUSSION

We found a good agreement between observed and Rietveld calculated PXRD patterns for both sample preparation methods. The improved Rietveld fit quality observed after iXAM addition to mineral mixtures (Table S1) likely originates from a reduced preferred orientation of crystalline minerals (Tsukimura 1997). Deteriorated fits at the upper end of iXAM contents (Table S1) were probably caused by increased background levels of the refined powder patterns, which decreased the integrated intensities and thus phase fractions associated with crystalline minerals (Gualtieri 2000). In contrast to previous studies (Chung 1974; Gualtieri 2000; Hillier 2000; Monecke et al. 2001; Chipera and Bish 2002, 2013), the quality of our Rietveld refinements was hardly affected by disordered clay minerals containing illite-smectite, kaolinite, and smectite, because suitable structure models accounting for stacking disorder (Ufer et al. 2004, 2008, 2012b, 2015) were readily available. However, we observed that the overestimation of disordered illite-smectite led to the underestimation of feldspars, but this did not affect the accuracy of quartz and calcite contents (Figs. 11 and S1, cp. Tables 2 and S1). Increasing overlap of peaks originating from amorphous materials and disordered clay minerals is likely to cause increasing deviations in Rietveld-derived mineral contents from their true values, especially when clay minerals (and feldspars) reach XRD detection and quantification limits (Hillier 1999b). Despite the incorporation of

548 mathematical algorithms for preferred orientation in many Rietveld software packages, reliable
549 results for crystalline minerals cannot always be assured (McCusker et al. 1999). Our results doc-
550 ument that the spherical harmonics algorithm provided by Bergmann et al. (2001) in Profex-
551 BGMN was able to provide a very good agreement between nominal and Rietveld-derived con-
552 tents of crystalline mineral phases (Figs. 10 and 11) and iXAMs (Fig. 5) in mineral mixtures.
553 Therefore, we found no significant difference between the conventional and spray-drying sample
554 preparation methods for the quantification of crystalline minerals and iXAMs in mineral mixtures
555 using Rietveld analysis. Spray drying slightly improved the precision of iXAM quantification and
556 is therefore preferable to the conventional sample preparation method when accounting for the
557 effects of preferred orientation of crystalline minerals (Bish and Reynolds 1989; Hillier 1999a,
558 2000). However, spray drying produced a higher precision variability as controlled by sample
559 complexity when compared to the conventional sample preparation method (Fig. 8). Generally,
560 QPA results from Rietveld analysis became less accurate with increasing contents of disordered
561 clay minerals, caused by the overlap of their broad diffraction peaks with the diffuse scattering
562 peaks of iXAMs.

563 So far, only few studies have provided results on the accuracy of Rietveld analyses for geo-
564 logical samples or mineral assemblages resembling geological or soil samples (Gualtieri 2000;
565 Hillier 2000; Monecke et al. 2001). Previous studies showed that the accuracy achieved by
566 Rietveld analysis is highly dependent on sample type and complexity (Bish and Post 1993; Hillier
567 2000; Monecke et al. 2001). With the Rietveld method, Hillier (2000) obtained an absolute error
568 of 10.2 wt% for the amorphous fraction (glass) in an artificial sandstone mixture, but achieved a
569 better result of 1.2 wt% for the same mixture using the RIR method. Similarly, a study on a family
570 of zeolite-rich sedimentary rock samples analyzed by the combined Rietveld-RIR method showed
571 deviations of 0.3–1.6 wt% for glass contents ranging between zero and 20 wt% (Gualtieri 2000).
572 At the 95 % confidence level, we achieved an average accuracy of ±3 wt% for both crystalline
573 minerals and iXAMs in mineral mixtures amended with 10–70 wt% iXAMs for both sample prep-

574 aration methods, which is identical to estimates of maximum uncertainties for crystalline minerals
575 following QPA of PXRD data published by Hillier (2000) for the RIR method and by Gualtieri
576 (2000) for the Rietveld-RIR method. Results of QPA of PXRD data with absolute errors within
577 ±3 wt% or 10 % relative error are generally considered 'highly accurate' or 'excellent' (Calvert et
578 al. 1989, Reynolds 1989). Including both sample preparation methods, we obtained a generalized
579 precision of iXAM quantification by the Rietveld method of ±2 wt% at the 95 % confidence level
580 and relative iXAM quantification errors < 10 % (except for one case; Fig. 7). Our data thus imply
581 that iXAMs in mineral mixtures can be accurately and precisely determined by Rietveld analysis
582 of PXRD patterns provided there are suitable crystallographic models for all crystalline minerals
583 in a given sample. For this, the internal standard quantity of 30 wt% proposed by Jones et al.
584 (2000) proved appropriate for the wide range of amorphous contents in our mineral mixtures.

585 Data on iXAM detection and quantification limits are not available in the literature. Our re-
586 sults indicate that soil iXAMs may not be accurately quantified by Rietveld analysis when present
587 at concentrations of less than about 4 wt%, but are already detectable at a 1 wt% level. These
588 numbers are almost certainly higher for real soils because crystalline mineral assemblages can be
589 much more complex than the mineral mixtures analyzed in this study and structure models for
590 crystalline minerals may not be appropriate or even available. In addition, organic matter, which
591 can dominate the amorphous fraction of soils, may not be completely removed prior to PXRD
592 analysis using H_2O_2, NaOCl, and $Na_2S_2O_8$ oxidants (Mikutta et al. 2005a) and thus significantly
593 contribute to the determined iXAM fraction at very low iXAM concentrations, particularly in soil
594 clay fractions (< 2 μm) of organic matter-rich soil horizons. In this respect, our iXAM quantifica-
595 tion results provide insight into what can be achieved by the Rietveld method under the best avail-
596 able conditions.

597 Based on Rietveld and XRF spectrometry results, the balance sheet method provided rea-
598 sonably accurate data on the chemical iXAM composition in terms of major oxides for both sam-
599 ple preparation methods, even at iXAM contents as low as 10 wt% (Figs. 14 and 15, Tables S10

and S12). This further buttresses the efficiency of Rietveld method in quantifying and characterizing the chemical composition of soil iXAMs based on XRF data. However, our results also show that the balance sheet method may significantly overestimate minor oxides (< 0.1 wt%) in iXAMs by up to 2.4 wt% (mean = 0.5 wt%) (Table S11). This was likely caused by small deviations between nominal and actual chemical compositions of crystalline minerals contained in the mineral mixtures and the intrinsic amorphicity or amorphicity induced in crystalline minerals during sample preparation. Therefore, oxide contents < 3 wt% determined for soil iXAMs are highly uncertain and should be viewed with due caution. In general, the mass bias of oxide contents (Al_2O_3, CaO, Fe_2O_3, K_2O, MgO, Na_2O, SiO_2, TiO_2) of up to ±3wt% derived from Rietveld and XRF analyses in our study was comparable to that obtained by full PXRD pattern fitting of soil samples combined with chemical analysis using inductively coupled plasma–mass spectrometry (Casetou-Gustafson et al. 2018).

The LOI of the ferrihydrite-opal mixture used in this study (15.3 wt%) contributed largely to the total LOI of all mineral mixtures analyzed (Table S9). This is a common phenomenon in soils, especially for iXAM-rich clay and silt fractions (Alexiades and Jackson 1966; Raman and Mortland 1969; Jones et al. 2000). Our results document that the balance sheet method leads to large relative LOI quantification errors of up to 371 % for the iXAMs used (mean = 67.2 %; Fig. 14, Table S12). This implies that LOI values determined for soil iXAMs become increasingly uncertain when iXAM contents are low and/or soil iXAMs possess an intrinsically low content of volatile elements such as ferrihydrite or opal-A (Fig. S3) as compared to, for example, short-range ordered aluminosilicates like allophane (Alexiades and Jackson 1966; Raman and Mortland 1969). Regardless of these restrictions, our results corroborate that the chemical composition of iXAMs in geomaterials in terms of major oxides can be accurately quantified using combined Rietveld and XRF analyses, irrespective of sample complexity and sample preparation method used for PXRD analysis.

IMPLICATIONS

Inorganic X-ray amorphous materials are a quantitatively important part of inorganic matter in soils (Blank and Fosberg 1991; Jones et al. 2000; Manaka 2006; Lessovaia et al. 2014, 2016), but analytical assessments of their quantification and chemical composition by QPA of PXRD data combined with chemical analyses are still lacking. Our results confirm that—independent of sample preparation method—Rietveld analysis can provide accurate and precise data on iXAM contents in mineral mixtures resembling soils and other geomaterials. However, this requires a correct identification and an accurate quantification of all crystalline mineral phases present, which still poses a major challenge for soils containing high amounts of disordered clay minerals.

Our established analytical parameters and limitations of the Rietveld method for the quantification and chemical characterization of iXAMs in artificial mineral mixtures provide indispensable information for the quantification and chemical characterization of iXAMs in natural soils. In fact, information on the distribution and composition of iXAMs in soils of most world regions is completely lacking, although a large number of studies have highlighted the importance of iXAMs for soil physicochemical properties such as organic carbon and pollutant binding, soil aggregation, porosity, and plasticity (Goldberg 1989; Mikutta et al. 2005b; Rawlins et al. 2013; Lehtinen et al. 2014; Totsche et al. 2018; Lenhardt et al. 2022). In soil sciences, iXAMs such as ferrihydrite, silica, and short-range ordered aluminosilicates like allophane or imogolite are almost exclusively quantified by selective wet-chemical dissolution methods (Higashi and Ikeda 1974; Taylor and Schwertmann 1974; Walker 1983; Parfitt and Childs 1988; Wada 1989; Kaufhold et al. 2010), but these methods are unable to assess the total abundance and chemical composition of soil iXAMs (Jones et al. 2000), especially when different kinds of iXAMs are present. QPA of PXRD data of soil samples in combination with elemental analysis on the other hand is currently the only method to reliably quantify total iXAM contents in soils and examine their chemical composition. This information is critical for establishing quantitative relationships between content and chemical

composition of iXAMs and physicochemical properties and ecological functions of soils in the future.

ACKNOWLEDGMENTS AND FUNDING

We are indebted to BGR for providing the minerals for this project and thank Claus Rüscher for assisting in the TG-DSC analyses. This work was funded by the German Research Foundation (DFG) (project no. 460744281).

REFERENCES

Abollino, O., Malandrino, M., Giacomino, A., and Mentasti, E. (2011) The role of chemometrics in single and sequential extraction assays: A review. Part I. Extraction procedures, uni- and bivariate techniques and multivariate variable reduction techniques for pattern recognition. Analytica Chimica Acta, 688, 104–121.

Ahtee, M., Nurmela, M., Suortti, P., and Järvinen, M. (1989) Correction for preferred orientation in Rietveld refinement. J. Appl. Cryst., 22, 261–268.

Alexiades, C.A., Jackson M.L. (1966) Quantitative clay mineralogical analysis of soils and sediments. Clays and Clay Minerals, 14, 35–52.

Andrist-Rangel, Y., Simonsson, M., Andersson, S., Öborn, I., and Hillier, S. (2006) Mineralogical budgeting of potassium in soil: a basis for understanding standard measures of reserve potassium. Journal of Plant Nutrition and Soil Sciences. 169, 605–615.

Basile-Doelsch, I., Balesdent, J., and Rose, J. (2015) Are interactions between organic compounds and nanoscale weathering minerals the key drivers of carbon storage in soils? Environmental Science and Technology, 49, 3997–3998.

Bazilevskaya, E., Archibald, D.D., and Martínez, C.E. (2018) Mineral colloids mediate organic carbon accumulation in a temperate forest Spodosol: depth-wise changes in pore water chemistry. Biogeochemistry, 141, 75–94.

Bergmann, J., Kleeberg, R., and Taut, T. (1997) Quantitative phase analysis using a new Rietveld algorithm – assisted by improved stability and convergence behavior. Advances in X-Ray Analysis, 40, 425.

Bergmann, J., Friedel, P., and Kleeberg, R. (1998) BGMN – a new fundamental parameters based Rietveld program for laboratory X-ray sources, its use in quantitative analysis and structure investigations. CPD Newslett., 20, 5–8.

Bergmann, J., Monecke, T., and Kleeberg, R. (2001) Alternative algorithm for the correction of preferred orientation in Rietveld analysis. J. Appl. Cryst., 34, 16–19.

Bish, D.L., and Post, J.E. (1993) Quantitative mineralogical analysis using the Rietveld full-pattern fitting method. American Mineralogist, 78, 932–940.

Bish, D.L., and Reynolds, R.C., Jr. (1989) "Sample Preparation for X-Ray Diffraction," In: D. L. Bish and J. E. Post, Eds., Modern Powder Diffraction. Mineralogical Society of America Reviews in Mineralogy, Washington DC, 20, 73–99.

Blank, R.R., and Fosberg, M.A. (1991) Duripans of Idaho, U.S.A.: In situ alteration of eolian dust (loess) to an opal-A/X-ray amorphous phase. Geoderma, 48, 131–149.

Brydon, J.E., and Shimoda, S. (1972) Allophane and other amorphous constituents in a podzol from Nova Scotia. Canadian Journal of Soil Science, 52, 465–475.

Calvert C.S., Palkowsky D.A., and Pevear D.R. (1989) A combined X-ray powder diffraction and chemical method for the quantitative mineral analysis of geological samples. Pp. 154–166 in: Quantitative Mineral Analysis of Clays (D.R Pevear & F.A, Mumpton, editors). Clay Minerals Society, Workshop Lectures, 5. Colorado, USA.

Casetou-Gustafson, S., Hillier, S., Akselsson, C., Simonsson, M., Stendahl, J., and Olsson, B.A. (2018) Comparison of measured (XRPD) and modeled (A2M) soil mineralogies: A study of some Swedish forest soils in the context of weathering rate predictions, Geoderma, 310, 77-88.

Cesarano, M., Bish, D.L., Cappelletti, P., Cavalcante, F., Belviso, C., and Fiore S. (2018) Quantitative mineralogy of clay-rich siliciclastic landslide terrain of the Sorrento Peninsula, Italy, using a combined XRPD and XRF approach. Clays and Clay Minerals 66, 353–369.

Chipera, S.J., and Bish, D.L. (2002) FULLPAT: A full-pattern quantitative analysis program for X-ray powder diffraction using measured and calculated patterns. Journal of Applied Crystallography, 35, 744–749.

Chipera, S.J., and Bish, D.L. (2013) Fitting full X-ray diffraction patterns for quantitative analysis: A method for readily quantifying crystalline and disordered phases. Advances in Materials Physics and Chemistry, 3, 47–53.

Chung, F.H. (1974) Quantitative interpretation of X-ray diffraction patterns of mixtures. I. Matrix-flushing method for quantitative multicomponent analysis. Journal of Applied Crystallography, 7, 519–525.

DeMumbrum, L.E. (1960) Crystalline and amorphous soil minerals of the Mississippi coastal terrace. Soil Science Society of America Journal, 24, 185–189.

Dietel, J., Gröger-Trampe, J., Bertmer, M., Kaufhold, S., Ufer, K., and Dohrmann, R. (2019a) Crystal structure model development for soil clay minerals – I. Hydroxy-interlayered smectite (HIS) synthesized from bentonite. A multi-analytical study. Geoderma, 347, 135–149.

Dietel, J., Ufer, K., Kaufhold, S., and Dohrmann, R. (2019b) Crystal structure model development for soil clay minerals – II. Quantification and characterization of hydroxy-interlayered smectite (HIS) using the Rietveld refinement technique. Geoderma, 347, 1–12.

Döbelin, N., and Kleeberg, R. (2015) Profex: a graphical user interface for the Rietveld refinement program BGMN. Journal of Applied Crystallography, 48, 1573–1580.

Dohrmann, R., Meyer, I., Kaufhold, S., Jahn, R., Kleber, M., and Kasbohm, J. (2002) Rietveld-based quantification of allophane. Mainzer Naturwissenschaftliches Archiv, 40, 28–30.

Dollase, W.A. (1986) Correction of intensities for preferred orientation in powder diffractometry: application of the March model. Journal of Applied Crystallography, 19, 267–272.

Filgueiras, A.V., Lavilla, I., and Bendicho, C. (2002) Chemical sequential extraction for metal partitioning in environmental solid samples. Journal of Environmental Monitoring, 4, 823–857.

Funk, W., Dammann, V., and Donnevert, G. (2005) Qualitätssicherung in der Analytischen Chemie. Wiley-VCH, Weinheim, 2nd ed.

Goldberg, S. (1989) Interaction of aluminum and iron oxides and clay minerals and their effect on soil physical properties: A review. Communications in Soil Science and Plant Analysis, 20, 1181–1207.

Gualtieri, A.F. (2000) Accuracy of XRPD QPA using the combined Rietveld RIR method. Journal of Applied Crystallography, 33, 267–278.

Gudmundsson, T., and Stahr, K. (1981) Mineralogical and geochemical alterations of "Podsol Bährhalde". Catena, 8, 49–69.

Hellmann, R., Eggleston, C.M., Hochella Jr., M.F., and Crerar, D.A. (1990) The formation of leached layers on albite surfaces during dissolution under hydrothermal conditions. Geochimica et Cosmochimica Acta, 54, 1267–1281.

Higashi, T., and Ikeda, H. (1974) Dissolution of allophane by acid oxalate solution. Clay Science, 4, 205–211.

Hillier, S. (1999a) Use of an air brush to spray dry samples for X-ray powder diffraction. Clay Minerals, 34, 127–135.

Hillier, S. (1999b) Quantitative analysis of clay and other minerals in sandstones by X-ray powder diffraction (XRPD). In R.H. Worden and S. Morad, Eds., Clay Mineral Cements in Sandstones pp. 213–251. Wiley.

Hillier, S. (2000) Accurate quantitative analysis of clay and other minerals in sandstones by XRD: Comparison of a Rietveld and a reference intensity ratio (RIR) method and the importance of sample preparation. Clay Minerals, 35, 291–302.

Järvinen, M. (1993) Application of symmetrized harmonics expansion to correction of the preferred orientation effect. Journal of Applied Crystallography, 26, 525–531.

Jones, R.C., Babcock, C.J., and Knowlton, W.B. (2000) Estimation of the total amorphous content of Hawai'i soils by the Rietveld method. Soil Science Society of America Journal, 64, 1100–1108.

Kaufhold, S., Ufer, K., Kaufhold, A., Stucki, J.W., Anastácio, A.S., Jahn, R., and Dohrmann, R. (2010) Quantification of allophane from Ecuador. Clays and Clay Minerals, 58, 707–716.

760 Kodama, H., and Wang, C. (1989) Distribution and characterization of non-crystalline inorganic
761 components in spodosols and spodosol-like soils. Soil Science Society of America Journal,
762 53, 526–534.

763 Lehtinen, T., Lair, G.J., Mentler, A., Gísladóttir, G., Ragnarsdóttir, K.V., and Blum, W.E.H.
764 (2014) Soil aggregate stability in different soil orders quantified by low dispersive ultra-
765 sonic energy levels. Soil Science Society of America Journal, 78, 713–723.

766 Lenhardt, K.R., Breitzke, H., Buntkowsky, G., Mikutta, C., and Rennert, T. (2022) Interactions of
767 dissolved organic matter with short-range ordered aluminosilicates by adsorption and co-
768 precipitation, Geoderma, 423, 115960.

769 Lessovaia, S., Dultz, S., Goryachkin, S., Plötze, M., Polekhovsky, Y., Andreeva, N., and Fili-
770 monov, A. (2014) Mineralogy and pore space characteristics of traprocks from Central Si-
771 beria, Russia: Prerequisite of weathering trends and soil formation. Applied Clay Science,
772 102, 186–195.

773 Lessovaia, S.N., Plötze, M., Inozemzev, S., and Goryachkin, S. (2016) Traprock transformation
774 into clayey materials in soil environments of the central Siberian plateau, Russia. Clays
775 and Clay Minerals, 64, 668–676.

776 Manaka, M. (2006) Amount of amorphous materials in relationship to arsenic, antimony, and bis-
777 muth concentrations in a brown forest soil. Geoderma, 136, 75–86.

778 McCusker, L.B., Von Dreele, R.B., Cox, D.E., Louër, D., and Scardi, P. (1999) Rietveld refine-
779 ment guidelines. Journal of Applied Crystallography, 32, 36–50.

780 Mikutta, R., Kleber, M., Kaiser, K., and Jahn, R. (2005a) Review: Organic matter removal from
781 soils using hydrogen peroxide, sodium hypochlorite, and disodium peroxodisulfate. Soil
782 Science Society of America Journal, 69, 120–135.

783 Mikutta, R., Kleber, M., and Jahn, R. (2005b) Poorly crystalline minerals protect organic carbon
784 in clay subfractions from acid subsoil horizons. Geoderma, 128, 106–115.

785 Monecke, T., Kohler, S., Kleeberg, R., Herzig, P.M., and Gemmell, J.B. (2001) Quantitative
786 phase-analysis by the Rietveld method using X-ray powder-diffraction data: Application to
787 the study of alteration Halos associated with volcanic rock hosted massive sulfide deposits.
788 The Canadian Mineralogist, 39, 1617–1633.

789 Omotoso, O., McCarty, D.K., Hillier, S., and Kleeberg, R. (2006) Some successful approaches to
790 quantitative mineral analysis as revealed by the 3rd Reynolds Cup contest. Clays Clay
791 Minerals, 54, 748–760.

792 Parfitt, R., and Childs, C. (1988) Estimation of forms of Fe and Al - a review, and analysis of con-
793 trasting soils by dissolution and Mossbauer methods. Soil Research, 26, 121–144.

794 Pospíšilová, Ľ., Uhlík, P., Menšík, L., Hlisnikovský, L., Eichmeier, A., Horáková, E., and Vlček,
795 V. (2021) Clay mineralogical composition and chemical properties of Haplic Luvisol de-
796 veloped on loess in the protected landscape area Litovelské Pomoraví. European Journal of
797 Soil Science, 72, 1128–1142.

798 Raman, K.V., and Mortland, M.M. (1969) Amorphous materials in a spodosol: Some mineralogi-
799 cal and chemical properties, Geoderma, 3, 37–43.

800 Rawlins, B.G., Wragg, J., and Lark, R.M. (2013) Application of a novel method for soil aggregate
801 stability measurement by laser granulometry with sonication. European Journal of Soil
802 Science, 64, 92–103.

803 Rennert, T. (2019) Wet-chemical extractions to characterise pedogenic Al and Fe species-a critical
804 review. Soil Research, 57, 1–16.

805 Rennert, T., Dietel, J., Heilek, S., Dohrmann, R., and Mansfeldt, T. (2021) Extraction of Al, Fe,
806 Mn, and Si from poorly crystalline and organic pedogenic species in sub-soil horizons by
807 (citrate-) ascorbate and oxalate. Geoderma, 397, 115095.

808 Reynolds, R.C., Jr. (1989) Principles and techniques of quantitative analysis of clay minerals by
809 X-ray powder diffraction. Pp. 4–36 in: Quantitative Mineral Analysis of Clays (D.R Pe-
810 vear & F.A. Mumpton, editors). Clay Minerals Society, Workshop Lectures, 1. Colorado,
811 USA.

812 Rietveld, H.M. (1969) A profile refinement method for nuclear and magnetic structures. Journal of
813 Applied Crystallography, 2, 65–71.

814 Ross, G.J. (1980) Mineralogical, physical, and chemical characteristics of amorphous constituents
815 in some podzolic soils from British Columbia. Canadian Journal of Soil Science, 60, 31–
816 43.

817 Ruiz-Agudo, E., Putnis, C.V., Rodriguez-Navarro, C., and Putnis, A. (2012) Mechanism of
818 leached layer formation during chemical weathering of silicate minerals. Geology, 40,
819 947–950.

820 Ruiz-Agudo, E., King, H.E., Patiño-Ĺopez, L.D., Putnis, C.V., Geisler, T., Rodriguez-Navarro, C.,
821 and Putnis, A. (2016) Control of silicate weathering by interface-coupled dissolution pre-
822 cipitation processes at the mineral-solution interface. Geology, 44, 567–570.

823 Sanborn, P., Lamontagne, L., and Hendershot, W. (2011) Podzolic soils of Canada: Genesis, dis-
824 tribution, and classification. Canadian Journal of Soil Science, 91, 843–880.

825 Scheffer, F., and Schachtschabel, P. (2010) Lehrbuch der Bodenkunde, 16th ed. (H.-P. Blume,
826 G.W. Brümmer, R. Horn, E. Kandeler, I. Kögel-Knabner, R. Kretzschmar, K. Stahr, & B.-
827 M. Wilke, Eds.). Spektrum Akademischer Verlag, Heidelberg.

828 Schwertmann, U., and Taylor, R.M. (1972) The transformation of lepidocrocite to goethite. Clays
829 and Clay Minerals, 20, 151–158.

830 Schwertmann, U., Schulze, D.G., and Murad, E. (1982) Identification of ferrihydrite in soils by
831 dissolution kinetics, differential X-ray diffraction, and Mössbauer spectroscopy. Soil Sci-
832 ence Society of America Journal, 46, 869–875.

833 Smith, S.T., Snyder, R.L., and Brownell, W.E. (1978) Minimization of preferred orientation in
834 powders by spray drying. Advances in X-Ray Analysis, 22, 77–87.

835 Szczerba, M., and Ufer, K. (2018) New model of ethylene glycol intercalate in smectites for XRD
836 modelling. Applied Clay Science, 153, 113–123.

Tamppari, L.K., Anderson, R.M., Archer Jr., P.D., Douglas, S., Kounaves, S.P., McKay, C.P., Ming, D.W., Moore, Q., Quinn, J.E., Smith, P.H., and others (2012) Effects of extreme cold and aridity on soils and habitability: McMurdo Dry Valleys as an analogue for the Mars Phoenix landing site. Antarctic Science, 24, 211–228.

Tarrah, J., Meiwes, K.J., and Meesenburg, H. (2000) Normative calculation of minerals in North German loess soils using the modified CIPW norm. Journal of Plant Nutrition and Soil Science, 163, 307–312.

Taylor, R.M., and Schwertmann, U. (1974) Maghemite in soils and its origin: I. Properties and observations on soil maghemites. Clay Minerals, 10, 289–298.

Totsche, K.U., Amelung, W., Gerzabek, M.H., Guggenberger, G., Klumpp, E., Knief, C., Lehndorff, E., Mikutta, R., Peth, S., Prechtel, A., and others (2018) Microaggregates in soils. Journal of Plant Nutrition and Soil Science, 181, 104–136.

Tsukimura, K. (1997) Crystallization of Al_2O_3–SiO_2 gels in water at 473K. Mineralogical Journal, 19, 1–11.

Ufer, K., Roth, G., Kleeberg, R., Stanjek, H., Dohrmann, R., and Bergmann, J. (2004) Description of X-ray powder pattern of turbostratically disordered layer structures with a Rietveld compatible approach. Zeitschrift für Kristallographie, 219, 519–527.

Ufer, K., Stanjek, H., Roth, G., Dohrmann, R., Kleeberg, R., and Kaufhold, S. (2008) Quantitative phase analysis of bentonites by the Rietveld method. Clays and Clay Minerals, 56, 272–282.

Ufer, K., Kleeberg, R., Bergmann, J., and Dohrmann, R. (2012a) Rietveld refinement of disordered illite-smectite mixed-layer structures by a recursive algorithm. I: One-dimensional patterns. Clays and Clay Minerals, 60, 507–534.

Ufer, K., Kleeberg, R., Bergmann, J., and Dohrmann, R. (2012b) Rietveld refinement of disordered illite-smectite mixed-layer structures by a recursive algorithm. II: Powder-pattern refinement and quantitative phase analysis. Clays and Clay Minerals, 60, 535–552.

Ufer, K., Kleeberg, R., and Monecke, T. (2015) Quantification of stacking disordered Si–Al layer silicates by the Rietveld method: application to exploration for high-sulphidation epithermal gold deposits. Powder Diffraction, 30, S111–S118.

Wada, K. (1989) Allophane and imogolite. In Minerals in soil environments pp. 1051–1087. Soil Science Society of America, Madison, WI.

Walker, A.L. (1983) The effects of magnetite on oxalate- and dithionite-extractable iron. Soil Science Society of America Journal, 47, 1022–1026.

Wang, X., Ufer, K., and Kleeberg, R. (2018) Routine investigation of structural parameters of dioctahedral smectites by the Rietveld method. Applied Clay Science, 163, 257–264.

Weidler, P.G., Luster, J., Schneider, J., Sticher, H., and Gehring, A.U. (1998) The Rietveld method applied to the quantitative mineralogical and chemical analysis of a ferralitic soil. European Journal of Soil Science, 49, 95–105.

875 Westphal, T., Füllmann, T., and Pöllmann, H. (2009) Rietveld quantification of amorphous por-
876 tions with an internal standard–Mathematical consequences of the experimental approach.
877 Powder Diffraction, 24, 239–243.

878 Zabala, S.M., Conconi, M.S., Alconada, M., and Torres Sánchez, R.M. (2007) The Rietveld meth-
879 od applied to the quantitative mineralogical analysis of some soil samples from Argentina.
880 Ciencia del Suelo, 25, 65–73.

881 Zahoransky, T., Kaiser, K., and Mikutta, C. (2022) High manganese redox variability and manga-
882 nate predominance in temperate soil profiles as determined by X-ray absorption spectros-
883 copy. Geochimica et Cosmochimica Acta, 338, 229–249.

884 Žigová, A., Šťastný, M., and Kodešová, A. (2013) Development of soils on paragneiss and granite
885 in the South-eastern part of Bohemia. Acta Geodynamica et Geomaterialia, 10, 85–95.

886

887 # FIGURE CAPTIONS

888 **Figure 1.** Scanning electron microscopy images of iXAMs used in this study (1:1 (w/w) mixture
889 of ferrihydrite and opal-A) before (a) and after (b) spray drying, (c) spray-dried mineral mixture B
890 with 40 wt% iXAMs, and (d) particle surface morphology of the spray-dried sample of mineral mixture B.
891 Scale bars in (a, d) are 1 μm and those in (b, c) 100 μm.

892 **Figure 2.** PXRD patterns of conventionally prepared ferrihydrite (Fhy), opal-A (Opl), and their
893 1:1 (w/w) mixture as well as the spray-dried mixture of ferrihydrite and opal-A.

894 **Figure 3.** PXRD patterns of mineral mixtures C (least complexity) and D (highest complexity)
895 after conventional sample preparation and spray drying. Cal = calcite; Chl = chlorite; Ilt-Sme =
896 illite-smectite; Kln = kaolinite; Qz = quartz.

897 **Figure 4.** Rietveld refinements of mineral mixture B containing 40 wt%. iXAMs after conven-
898 tional sample preparation (top) and spray drying (bottom).

899 **Figure 5.** Linear relationships between nominal and Rietveld-derived iXAM contents of mineral
900 mixtures A–D amended with 10–70 wt% iXAMs after conventional sample preparation and spray
901 drying (data uncorrected for the initial amorphous content of mineral mixtures).

Figure 6. Frequency distribution of absolute iXAM quantification errors for mineral mixtures A–D amended with 10–70 wt% iXAMs after conventional sample preparation and spray drying (data corrected for the initial amorphous content of mineral mixtures).

Figure 7. Relative iXAM quantification errors for mineral mixtures A–D amended with 10–70 wt% iXAMs after conventional sample preparation and spray drying (data corrected for the initial amorphous content of mineral mixtures). The regression line applies to all data.

Figure 8. Boxplots illustrating the precision of iXAM quantification for mineral mixtures B–D amended with 10 wt% iXAMs (N = 5 for each mixture) after conventional sample preparation and spray drying (data corrected for the initial amorphous content of mineral mixtures). The boxes contain 50 % of the data (interquartile range, IQR). The middle line represents the median (50^{th} percentile). Whiskers include data within 1.5 × IQR. Different uppercase letters indicate significant differences between each mineral mixture prepared either conventionally or by spray drying, and different lowercase letters indicate significant differences between all mineral mixtures for each sample preparation method.

Figure 9. Linear calibration function of nominal versus Rietveld-derived iXAM contents of spray-dried mineral mixture B amended with 1–10 wt% iXAMs (data corrected for the initial amorphous content of the mineral mixture).

Figure 10. Plots of nominal versus Rietveld-derived contents of crystalline non-clay and clay minerals in mineral mixture C amended with 0–70 wt% iXAMs after conventional sample preparation and spray drying. Cal = calcite; Chl = chlorite; Ilt-Sme = illite-smectite; Or = orthoclase; Qz = quartz.

Figure 11. Plots of nominal versus Rietveld-derived contents of crystalline non-clay and clay minerals in mineral mixture D amended with 0–70 wt% iXAMs after conventional sample preparation and spray drying. Chl = chlorite; Ilt-Sme = illite-smectite; Kln = kaolinite; Lb = labradorite; Or = orthoclase; Qz = quartz; Sme = smectite.

Figure 12. Frequency distribution of absolute quantification errors for crystalline mineral phases in mineral mixtures A–D amended with 0–70 wt% iXAMs after conventional sample preparation and spray drying. The red lines show fits of Gaussian functions and are meant to guide the eye.

Figure 13. Comparison of XRF- and Rietveld-derived chemical compositions of initial mineral mixtures A–D after conventional sample preparation and spray drying.

Figure 14. Comparison of nominal and mass balance-derived iXAM contents of SiO_2, Fe_2O_3, and LOI and their relative errors for mineral mixtures B–D amended with 10–70 wt% iXAMs afterconventional sample

preparation and spray drying. Nominal oxide contents were determined by XRF spectrometry. Gray shaded areas mark the ±10 % error margin.

Figure 15. Regression of nominal and mass balance-derived sums of SiO_2, Fe_2O_3, and LOI in iXAMs for mineral mixtures B–D amended with 10–70 wt% iXAMs after conventional sample preparation and spray drying. Nominal oxide contents were determined by XRF spectrometry.

Tables

Table 1. Description of minerals used in this study.

Mineral	Source	Nominal formula	Purity (%)[a]
Albite (Ab)	Tørdal, Norway	$NaAlSi_3O_8$	94.3
Calcite (Cal)	Hunan, China	$CaCO_3$	100
Chlorite (Chl)	Korshunovskaia mine, Russia	$(Mg, Fe^{2+})_5Al\,(Si_3Al)\,O_{10}(OH)_8$	100
Corundum Baikalox CR1 (Crn)	Baikowski (synthetic)	Al_2O_3	100
Ferrihydrite (Fhy)	Own lab (synthetic)	$Fe_2O_3{\cdot}9H_2O$	100
Illite-smectite, disordered (Ilt-Sme)[b]	Korom Hill, Hungary	$(Ca,K)\,(Al, Mg, Fe)_2\,(Si, Al)_4O_{10}\,(OH)_2$	96.9
Kaolinite, disordered (Kln)	Mauretania	$Al_2Si_2O_5(OH)_4$	97.0
Labradorite (Lb)	Bekily, Madagascar	$(Ca,Na)(Si,Al)_4O_8$	100
Opal-A (Opl)	China (synthetic)	$SiO_2{\cdot}11H_2O$	100
Orthoclase (Or)[c]	Stavern, Norway	$(K,Na)(Al,Si)_4O_8$	100
Quartz (Qz)	Unknown	SiO_2	100
Smectite, disordered (Sme)[d]	Milos, Greece	$(Al, Fe, Mg)_2\,(Si, Al)_4O_{10}(OH)_2$	93.2

[a]Without intrinsic or induced amorphicity during sample preparation. Minor phases: Ab, 5.7 % quartz; Ilt-Sme, 3.1 % quartz; Sme, 3.5 % orthoclase and 3.3 % albite; Kln, 2 % anatase, < 1 % quartz, < 1 % rutile, and < 1 % svanbergite.

[b]Illite-smectite mixed-layer mineral with R3 ordering with traces of quartz similar to the illite-smectite F4 sample in Ufer et al. (2012b).

[c]Mixture of K and Na feldspars (microcline and plagioclase 16an).

[d]Smectite-dominated (93.2 %) bentonite with traces of feldspars (Ufer et al. 2008).

Table 2. Mineral mixtures and their respective compositions (wt%).

Mixture[a]	Qz	Feldspars			Cal	Chl	Ilt-Sme	Kln	Sme
		Ab	Lb	Or					
A	60	10	-	10	-	5	10	5	-
B	50	10	-	10	10	-	15	5	-
C	40	-	-	15	20	5	20	-	-
D	20	-	10	20	-	5	20	15	10

[a] A: loess composition without calcite, B: loess composition with calcite, C: composition of a marly glacial till, D: granite composition. Ab = albite; Cal = calcite; Chl = chlorite; Ilt-Sme = illite-smectite; Kln = kaolinite; Lb = labradorite; Or = orthoclase; Qz = quartz; Sme = smectite.

971

972

973

974

975

976

977

978

979

Table 3. Comparison between nominal and Rietveld-derived iXAM contents (wt%) for mineral mixtures A–D after conventional sample preparation and spray drying with estimated standard deviations (e.s.d.) as well as absolute (wt%) and relative (%) quantification errors. Rietveld-derived iXAM contents were corrected for the initial amorphous content of mineral mixtures.

	Conventional				Spray-dried			
Nominal	**Rietveld**	**e.s.d.**	**Abs. error**	**Rel. error**	**Rietveld**	**e.s.d.**	**Abs. error**	**Rel. error**
				Mixture A				
10	11.33	0.27	1.33	13.3	9.43	0.23	-0.57	5.71
20	19.40	0.29	-0.60	3.02	21.11	0.23	1.11	5.54
30	30.75	0.27	0.75	2.51	29.65	0.22	-0.35	1.18
40	38.50	0.29	-1.50	3.74	40.59	0.22	0.59	1.47
50	48.57	0.26	-1.43	2.86	48.94	0.23	-1.07	2.13
60	58.03	0.26	-1.97	3.29	58.01	0.20	-1.99	3.31
70	68.17	0.22	-1.83	2.62	68.50	0.17	-1.50	2.14
				Mixture B				
10	10.81	0.26	0.81	8.14	10.37	0.22	0.37	3.72
20	20.17	0.25	0.17	0.84	20.72	0.23	0.72	3.62
30	31.97	0.25	1.97	6.57	30.74	0.22	0.74	2.45
40	40.13	0.25	0.13	0.31	40.90	0.21	0.90	2.24
50	50.79	0.24	0.79	1.58	51.73	0.22	1.73	3.46
60	61.09	0.20	1.09	1.82	61.71	0.20	1.71	2.85
70	69.63	0.21	0.37	0.53	70.60	0.17	0.60	0.86
				Mixture C				
10	9.91	0.27	-0.09	0.87	10.23	0.23	0.23	2.33
20	21.83	0.26	1.83	9.13	20.96	0.24	0.96	4.78
30	30.63	0.26	0.63	2.10	29.49	0.22	-0.51	1.70
40	41.89	0.23	1.89	4.73	41.14	0.20	1.14	2.85
50	51.26	0.22	1.77	2.51	51.80	0.22	1.80	3.59
60	61.77	0.22	1.77	2.95	61.80	0.19	1.80	3.00
70	69.51	0.22	-0.49	0.70	69.32	0.20	-0.68	0.97
				Mixture D				
10	10.05	0.32	0.04	0.45	9.85	0.23	-0.15	1.52
20	18.80	0.28	-1.20	6.00	20.09	0.25	0.09	0.43

30	28.84	0.30	-1.17	3.88	31.15	0.22	1.15	3.85
40	38.49	0.27	-1.51	3.78	39.10	0.23	-0.90	2.24
50	49.54	0.26	-0.47	0.93	48.65	0.22	-1.35	2.70
60	61.24	0.23	1.24	2.07	58.46	0.20	-1.54	2.57
70	69.62	0.22	-0.38	0.55	69.49	0.19	-0.51	0.73

Table 4. Absolute (wt%) and relative errors (%) of iXAM quantification by mineral mixture after conventional sample preparation and spray drying.

		Conventional		**Spray-dried**	
Mixture		**Abs. error**	**Rel. error**	**Abs. error**	**Rel. error**
A	Mean	-0.75	4.48	-0.54	3.07
	2σ	2.61	7.81	2.21	3.75
B	Mean	0.76	2.83	0.97	2.75
	2σ	1.29	6.34	1.08	2.02
C	Mean	1.04	3.28	0.68	2.75
	2σ	2.03	5.83	2.04	2.50
D	Mean	-0.49	2.52	-0.46	2.01
	2σ	1.88	4.20	1.85	2.39
Total[a]	Mean	0.14	3.28	0.16	2.64
	2σ	2.47	6.02	2.21	2.70
General[b]	Mean	0.15	2.96		
	2σ	2.32	4.67		

[a] For all mixtures of each sample preparation method.

[b] For all mixtures and both sample preparation methods.

Table 5. Example balance sheet calculation for the assignment of oxides (X-ray fluorescence data given in parentheses) to the iXAM fraction of spray-dried mineral mixture B containing 40 wt% iXAMs. All values are given in wt%.

Mineral[a]	**Oxides**										
	SiO_2 (60.61)	**TiO_2 (0.08)**	**Al_2O_3 (6.24)**	**Fe_2O_3 (17.35)**	**MgO (0.20)**	**CaO (3.51)**	**Na_2O (1.01)**	**K_2O (1.11)**	**LOI**[b] **(9.66)**	**Total (99.77)**	**Rietveld**[c]
Ab	3.20	-	1.02	-	-	-	0.58	-	-		4.78(16)
Cal	-	-	-	-	-	2.74	-	-	2.14		4.87(3)
Or	3.18	-	1.02	-	-	0.09	0.27	0.38	-		4.97(12)
Qz	28.52	-	-	-	-	-	-	-	-		28.52(8)
Ilt-Sme	6.31	-	2.52	0.24	0.71	-	-	1.10	-		10.88(13)
Kln	1.50	-	1.27	-	-	-	-	-	-		2.77(5)
iXAMs[d]	17.90	0.08	0.41	17.11	-0.51	0.69	0.17	-0.36	7.52	43.12	43.25(24)

[a] Mineral abbreviations: Ab = albite; Cal = calcite; Ilt-Sme = illite-smectite; Kln = kaolinite; Or = orthoclase; Qz = quartz.

[b] Loss on ignition.

[c] Standard deviations (σ) in parentheses apply to the last digit.

[d] Nominal oxide and LOI contents of iXAMs in mineral mixture (wt%): SiO_2 = 16.51, Fe_2O_3 = 17.22, and LOI = 6.13.

Figure 1

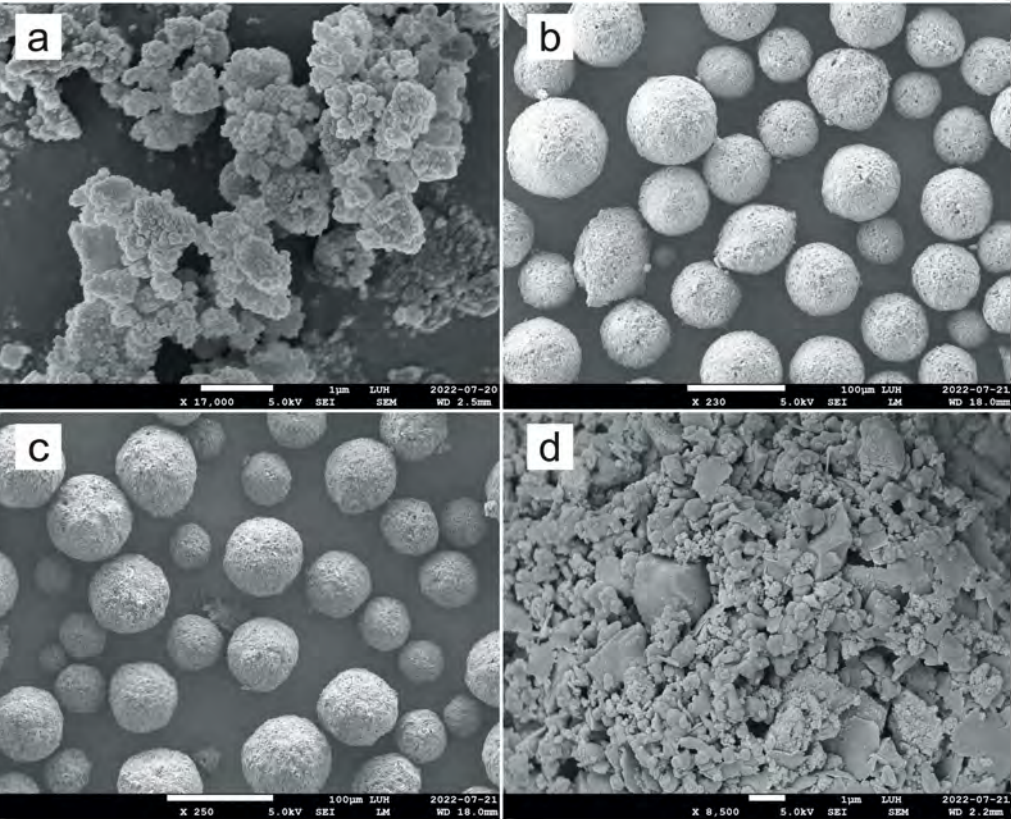
a
1µm LUH 2022-07-20
X 17,000 5.0kV SEI SEM WD 2.5mm
b
100µm LUH 2022-07-21
X 230 5.0kV SEI LM WD 18.0mm
c
100µm LUH 2022-07-21
X 250 5.0kV SEI LM WD 18.0mm
d
1µm LUH 2022-07-21
X 8,500 5.0kV SEI SEM WD 2.2mm

Figure 2

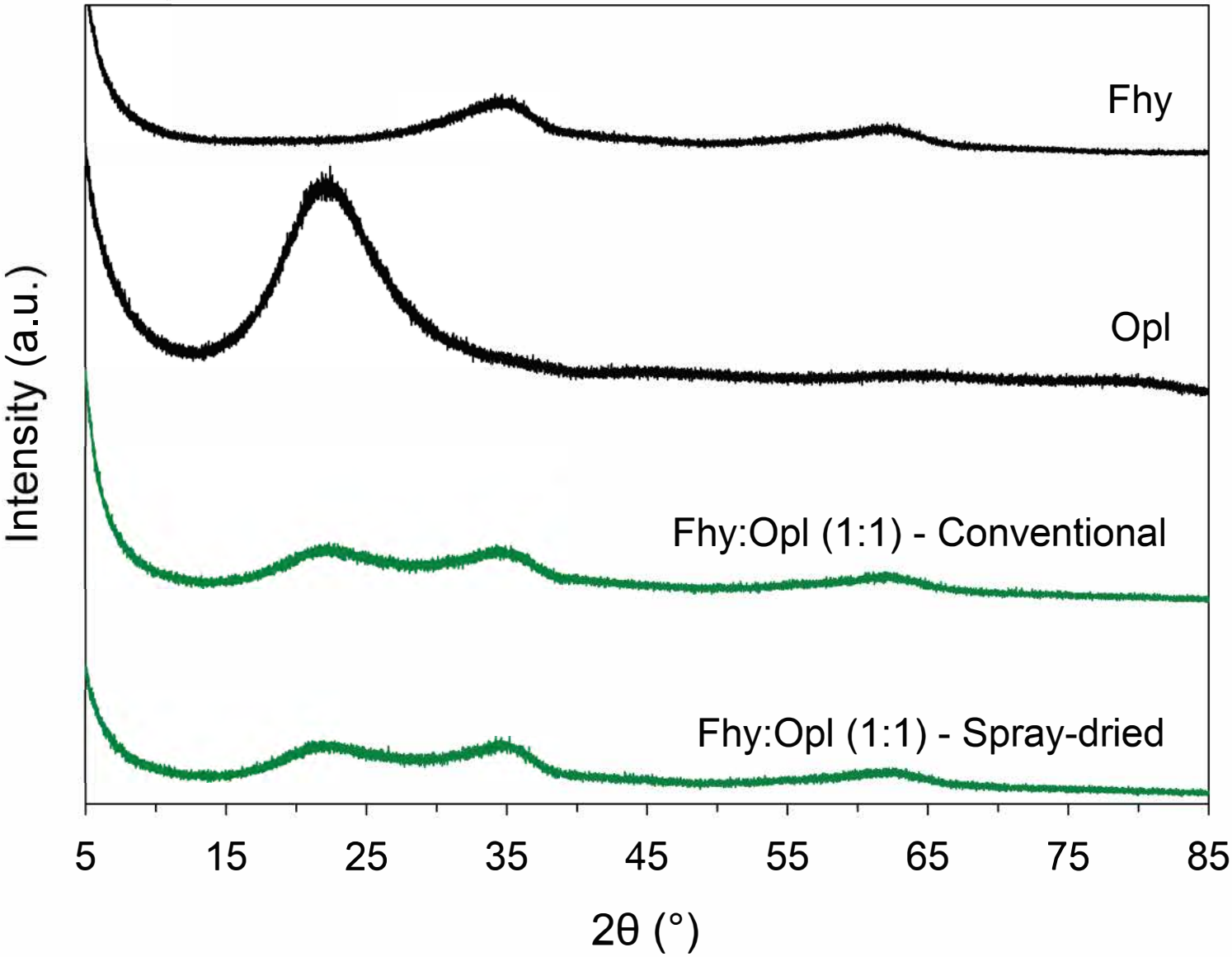
Fhy
Opl
Fhy:Opl (1:1) - Conventional
Fhy:Opl (1:1) - Spray-dried
Intensity (a.u.)
5
15
25
35
45
55
65
75
85
2θ (°)

Figure 3

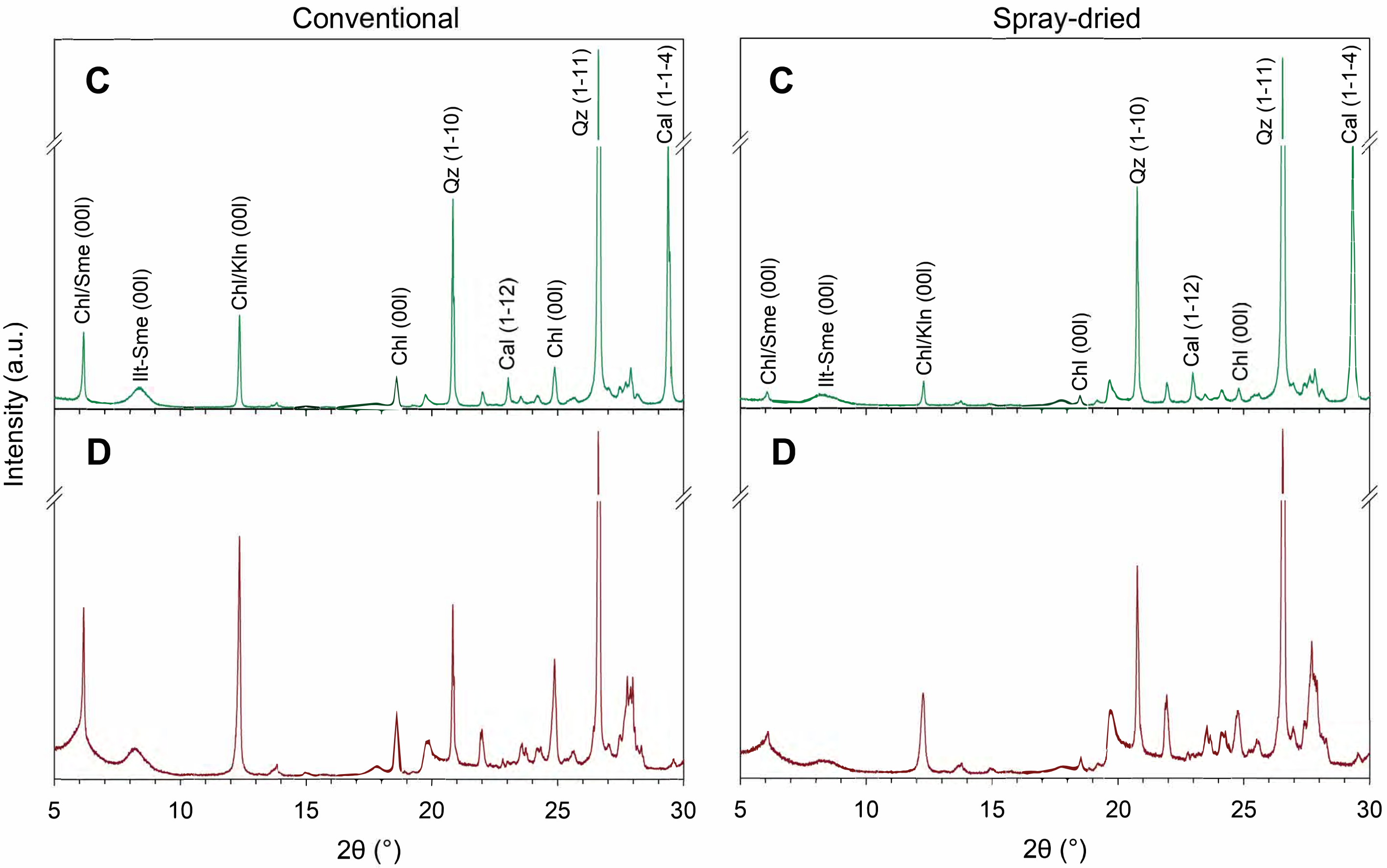
Conventional
Spray-dried
c
D
Chl/Sme (00l)
Ilt-Sme (00l)
Chl/Kln (00l)
Chl (00l)
Qz (1-10)
Cal (1-12)
Chl (00l)
Qz (1-11)
Cal (1-1-4)
Intensity (a.u.)
5
10
15
20
25
30
2θ (°)

Figure 4

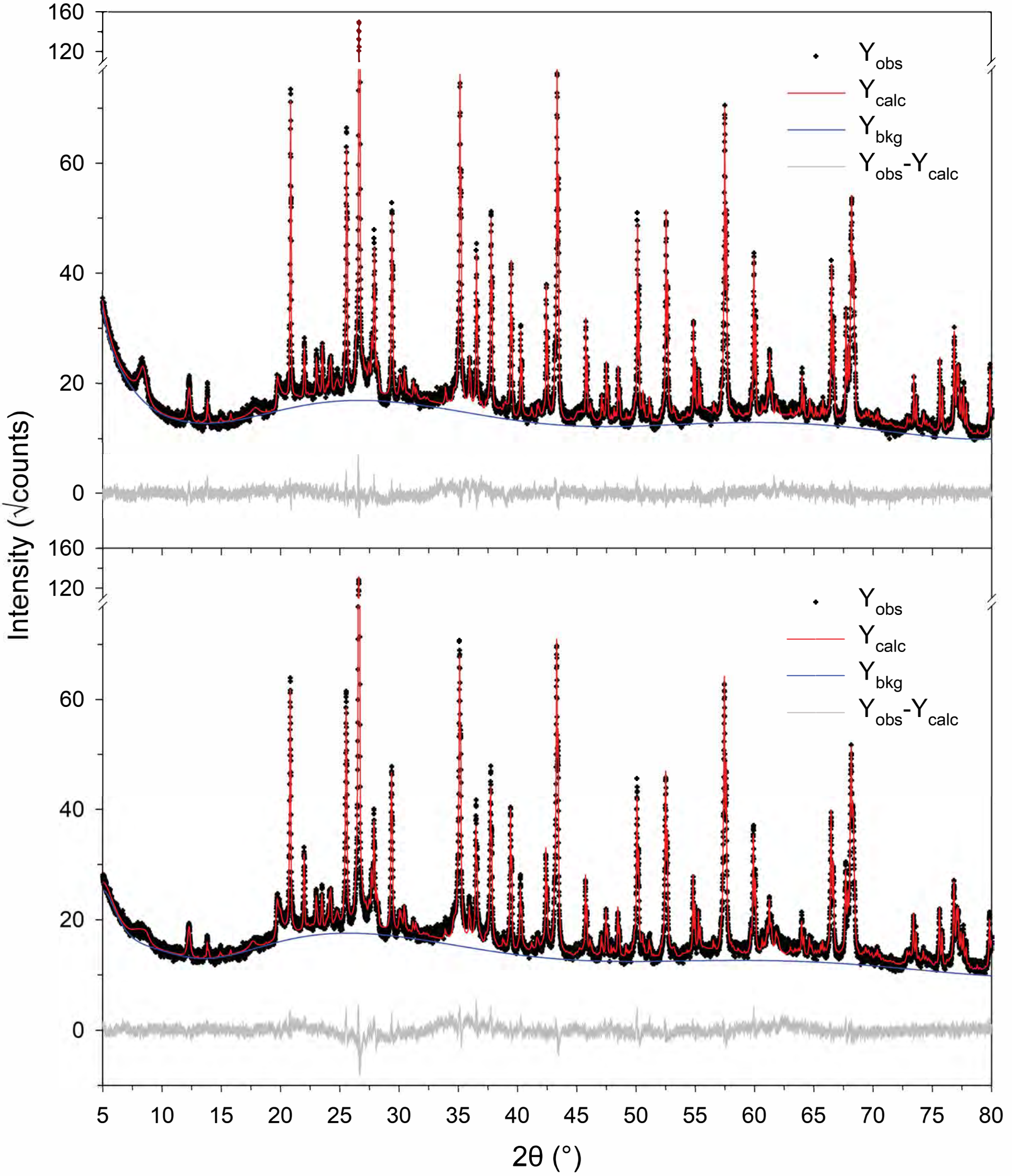
Intensity (√counts)
160
120
60
40
20
0
Y obs
Y calc
Y bkg
Y obs-Y calc
5
10
15
20
25
30
35
40
45
50
55
60
65
70
75
80
2θ (°)

Figure 5

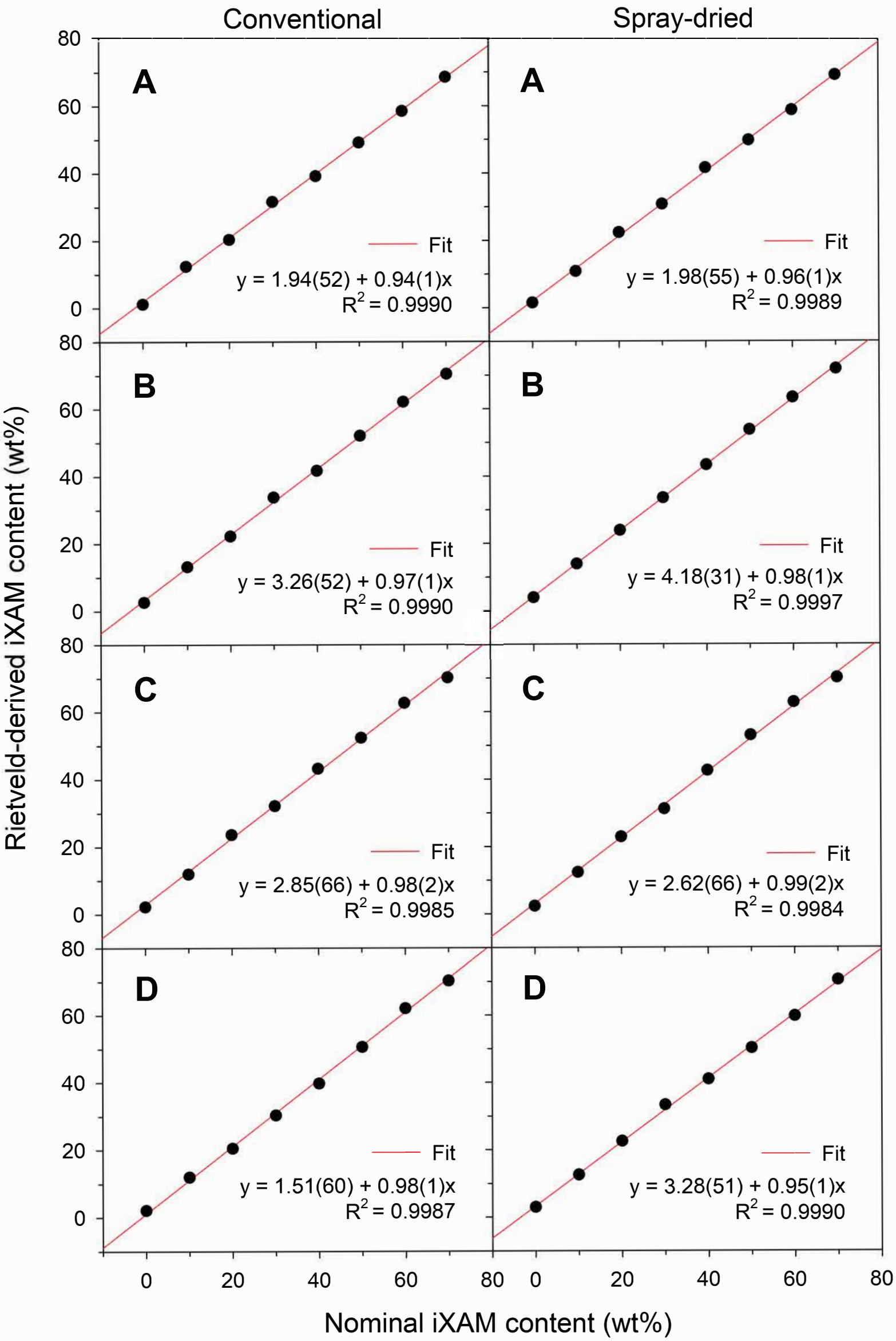
Conventional
Spray-dried
A
B
C
D
Fit
y = 1.94(52) + 0.94(1)x
R2 = 0.9990
y = 1.98(55) + 0.96(1)x
R2 = 0.9989
y = 3.26(52) + 0.97(1)x
R2 = 0.9990
y = 4.18(31) + 0.98(1)x
R2 = 0.9997
y = 2.85(66) + 0.98(2)x
R2 = 0.9985
y = 2.62(66) + 0.99(2)x
R2 = 0.9984
y = 1.51(60) + 0.98(1)x
R2 = 0.9987
y = 3.28(51) + 0.95(1)x
R2 = 0.9990
0
20
40
60
80
Rietveld-derived iXAM content (wt%)
Nominal iXAM content (wt%)

Figure 6

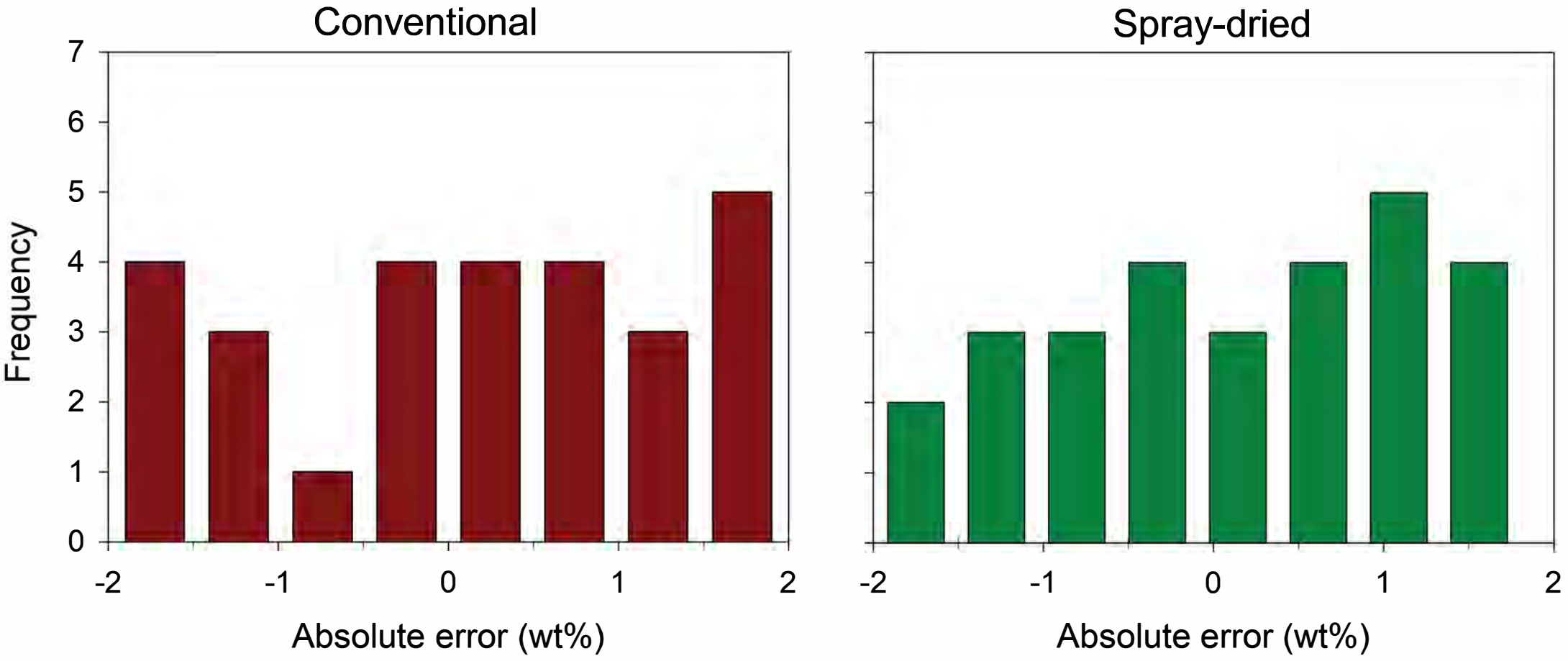
Conventional
Spray-dried
Frequency
0
1
2
3
4
5
6
7
-2
-1
0
1
2
Absolute error (wt%)
Absolute error (wt%)

Figure 7

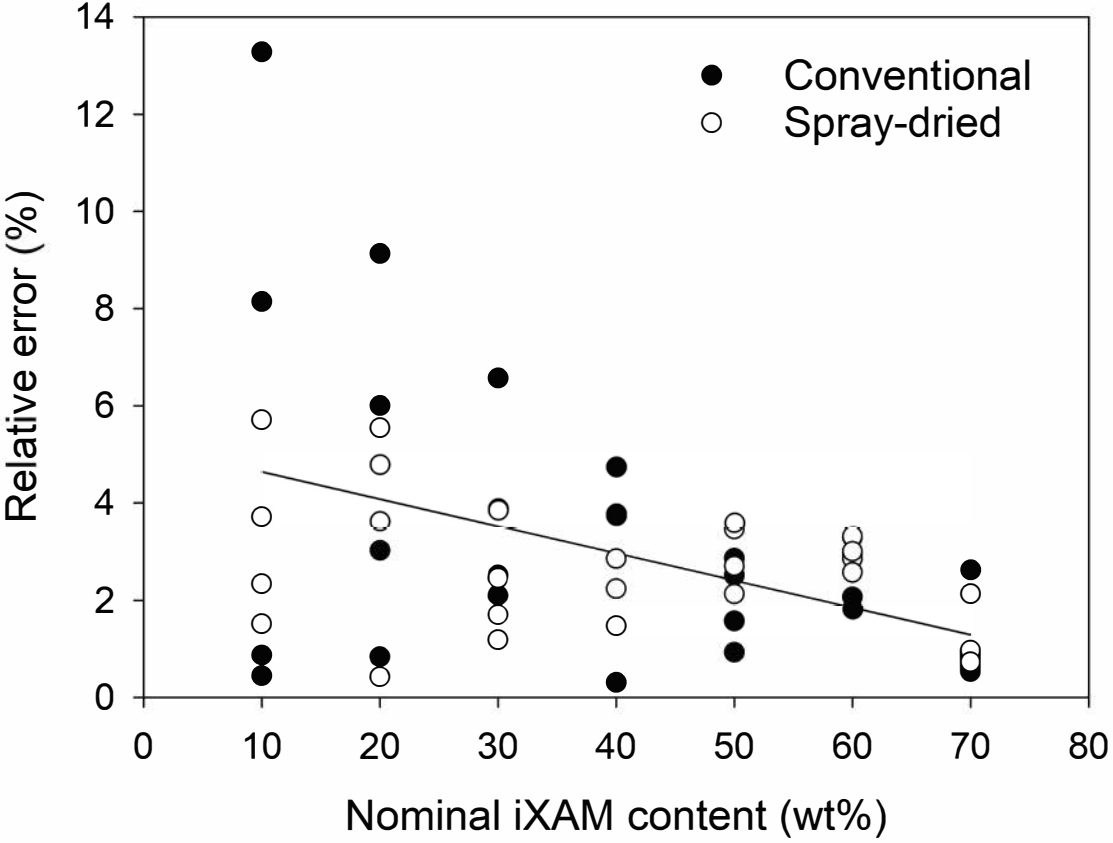
Conventional
Spray-dried
Relative error (%)
Nominal iXAM content (wt%)
0
2
4
6
8
10
12
14
0
10
20
30
40
50
60
70
80

Figure 8

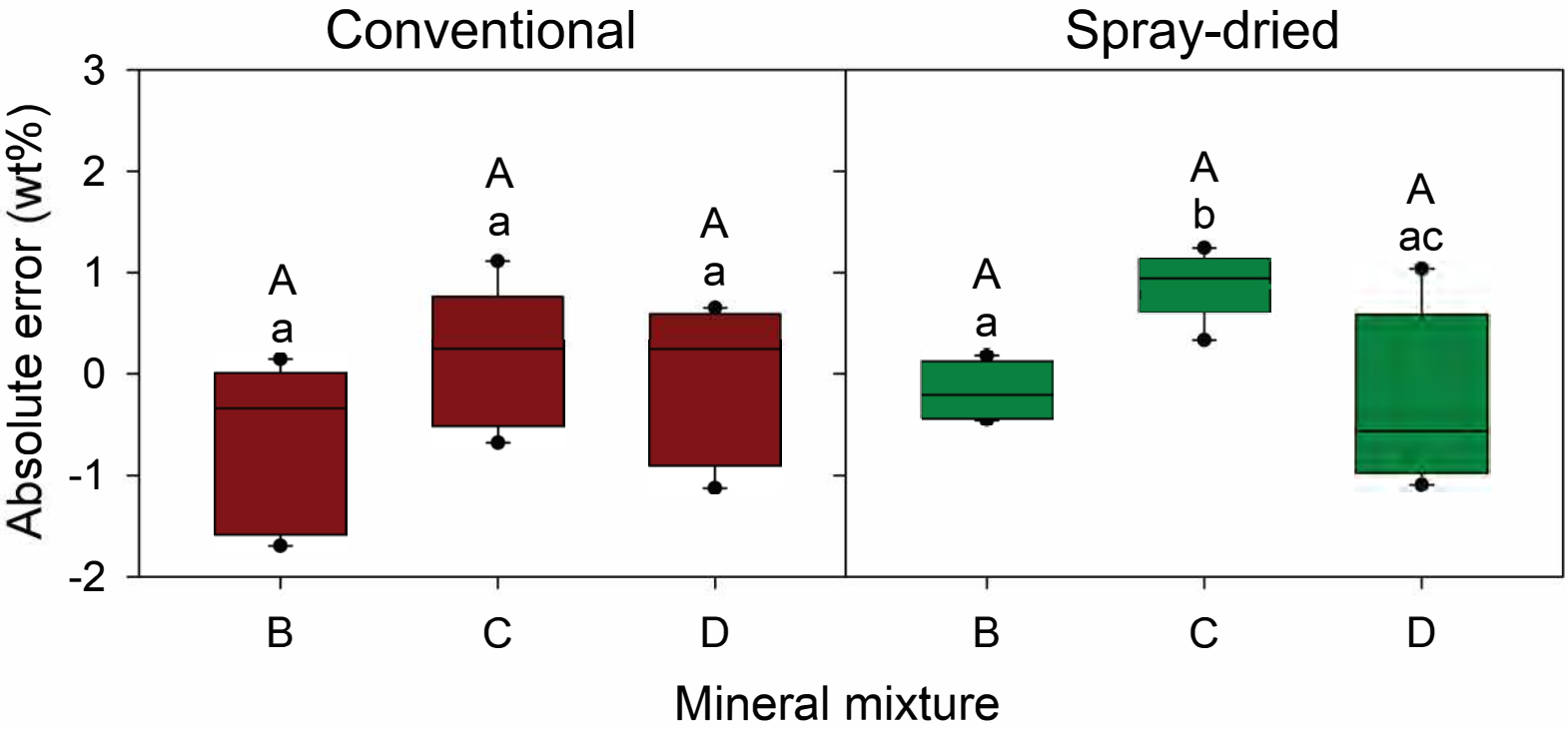
Conventional
Spray-dried
Absolute error (wt%)
3
2
1
0
-1
-2
A
a
A
a
A
a
A
a
A
b
A
ac
B
C
D
B
C
D
Mineral mixture

Figure 9

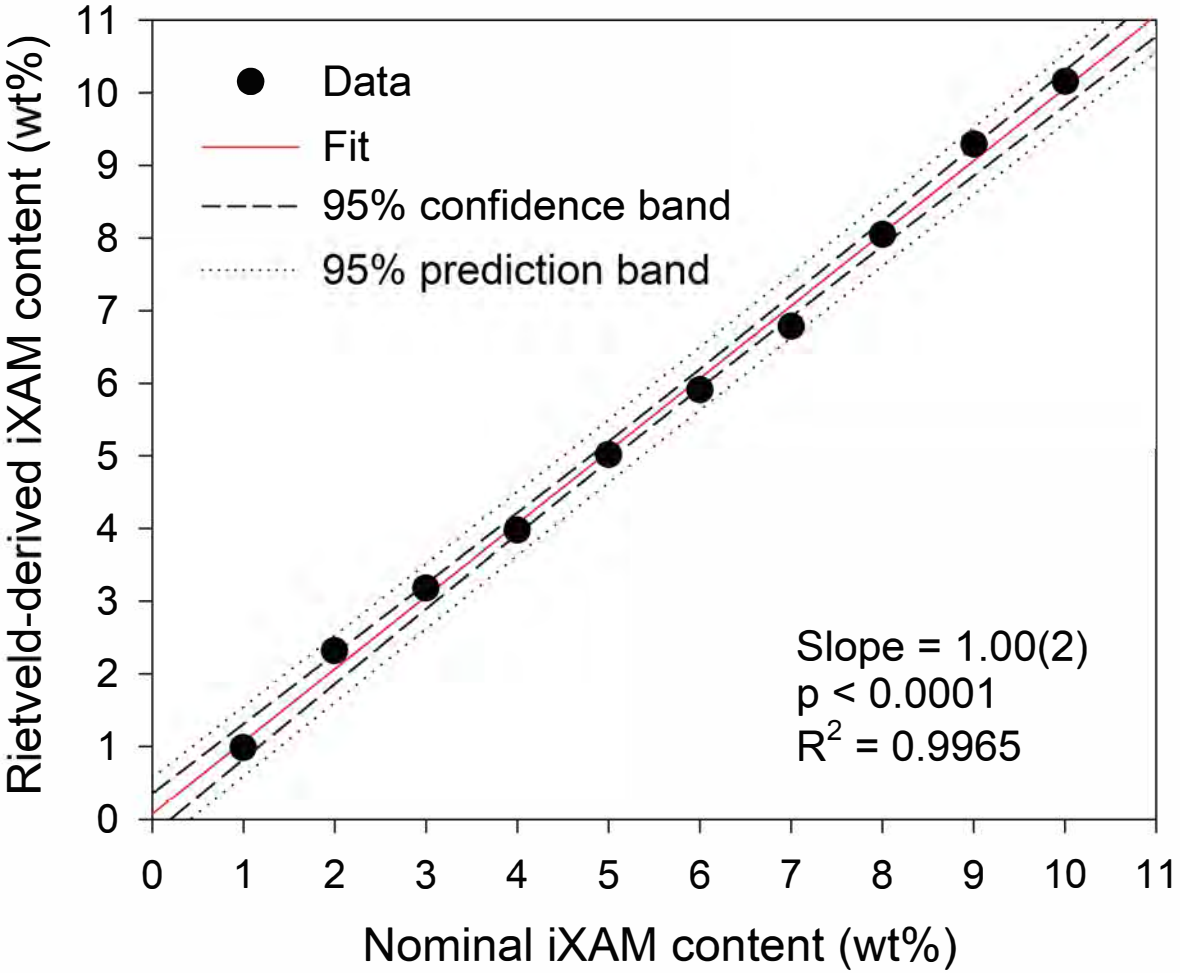
Data
Fit
95% confidence band
95% prediction band
Slope = 1.00(2)
p < 0.0001
R2 = 0.9965
Rietveld-derived iXAM content (wt%)
Nominal iXAM content (wt%)
0
1
2
3
4
5
6
7
8
9
10
11

Figure 10

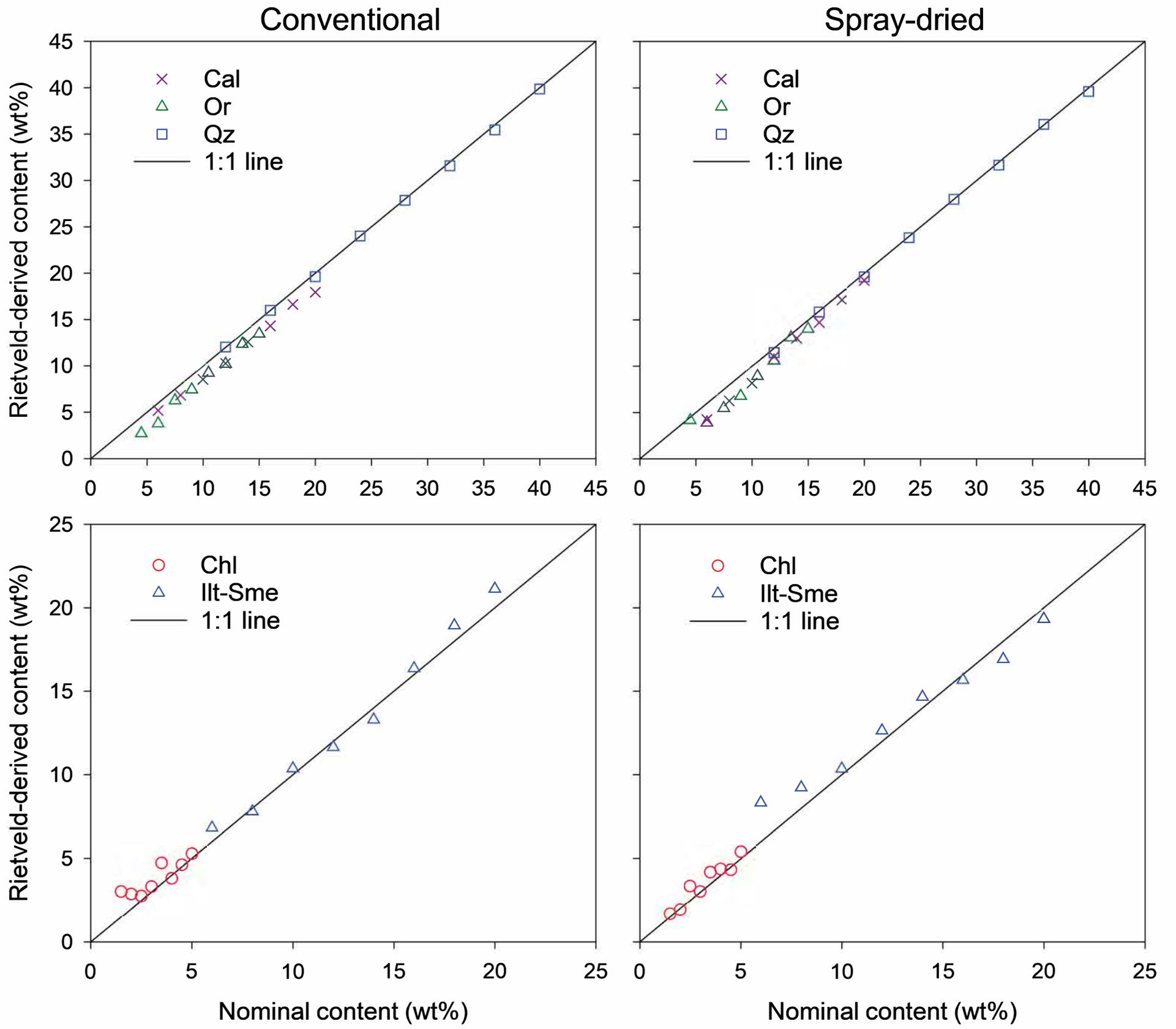
Conventional
Spray-dried
Cal
Or
Qz
1:1 line
Chl
Ilt-Sme
1:1 line
Rietveld-derived content (wt%)
Nominal content (wt%)
0
5
10
15
20
25
30
35
40
45

Figure 11

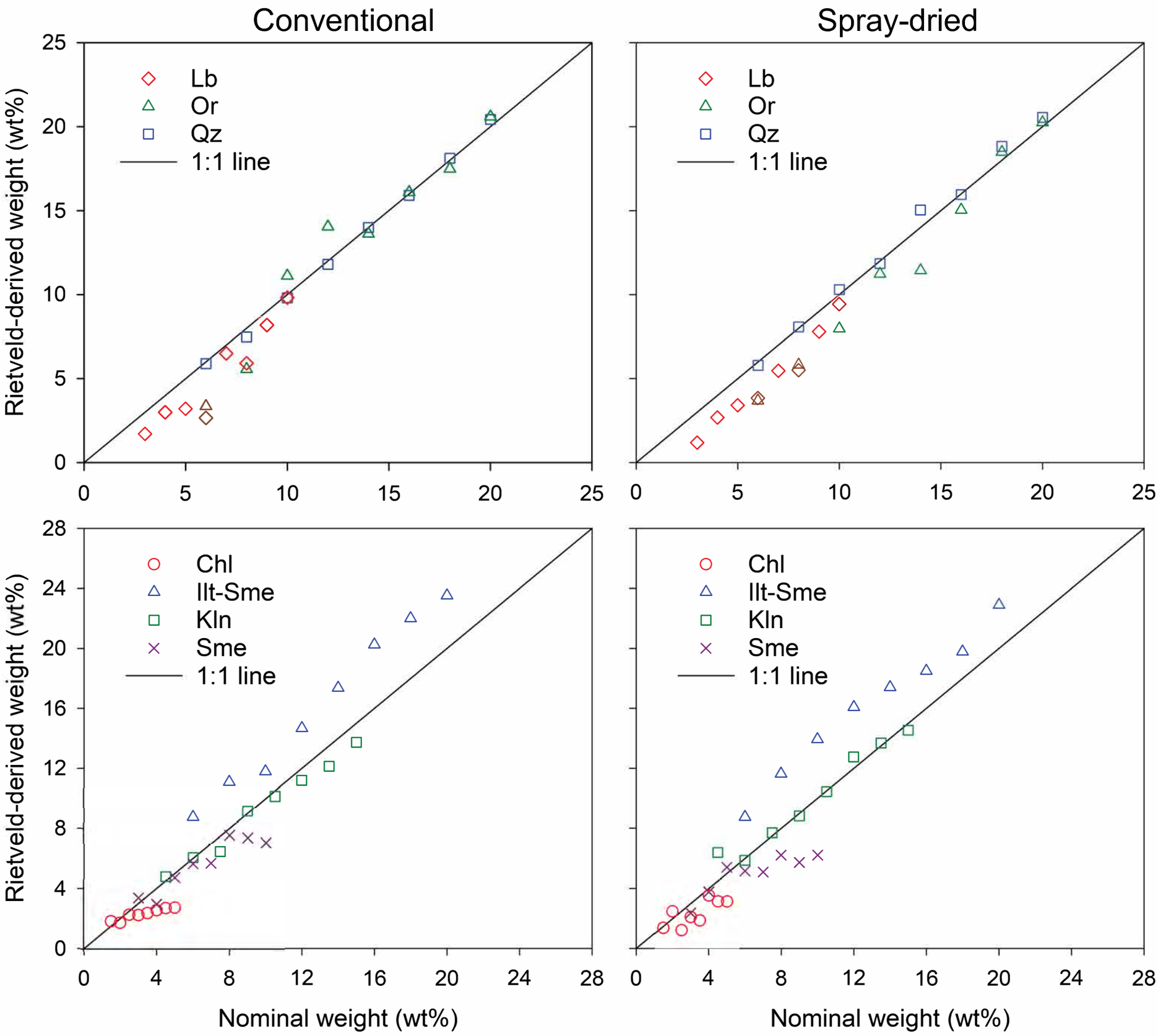
Conventional
Spray-dried
Lb
Or
Qz
1:1 line
Chl
Ilt-Sme
Kln
Sme
Rietveld-derived weight (wt%)
Nominal weight (wt%)
0
5
10
15
20
25
0
4
8
12
16
20
24
28

Figure 12

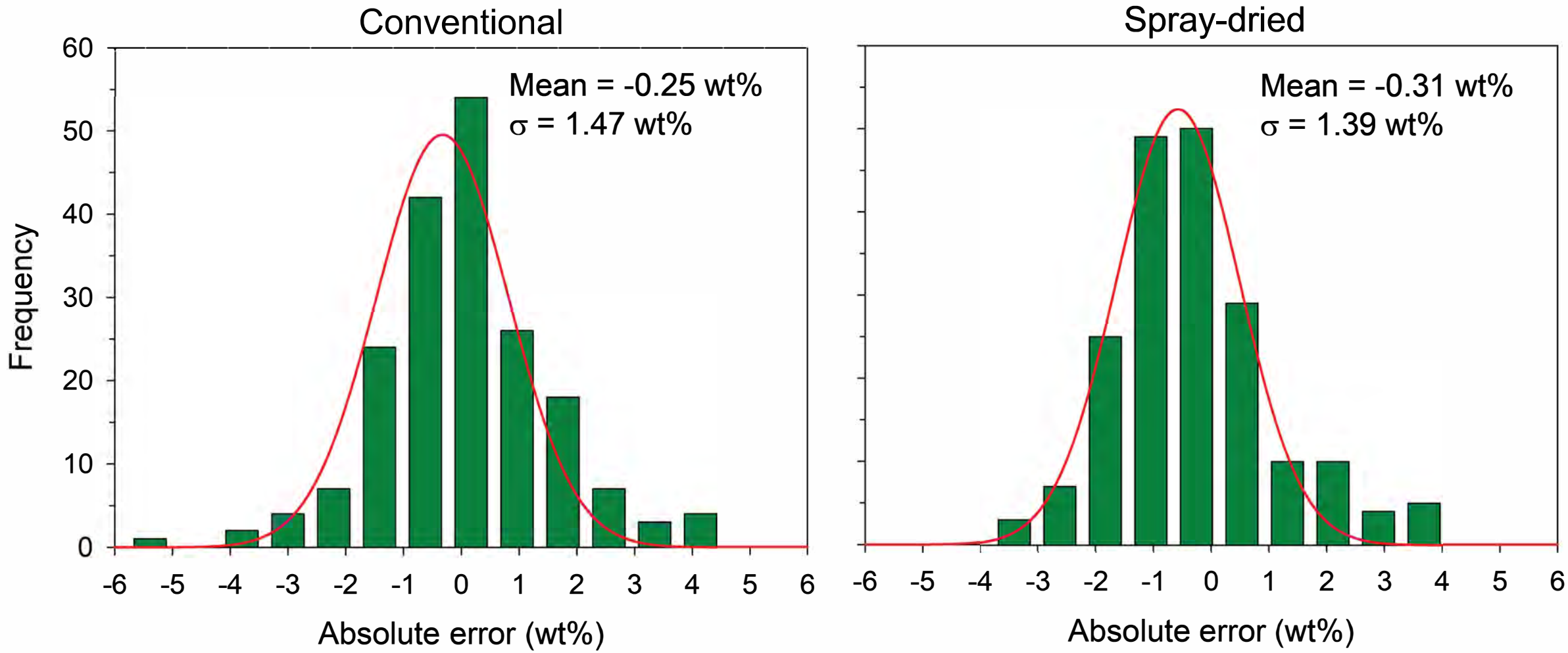
Conventional
Mean = -0.25 wt%
σ = 1.47 wt%
Frequency
60
50
40
30
20
10
0
-6 -5 -4 -3 -2 -1 0 1 2 3 4 5 6
Absolute error (wt%)
Spray-dried
Mean = -0.31 wt%
σ = 1.39 wt%
-6 -5 -4 -3 -2 -1 0 1 2 3 4 5 6
Absolute error (wt%)

Figure 13

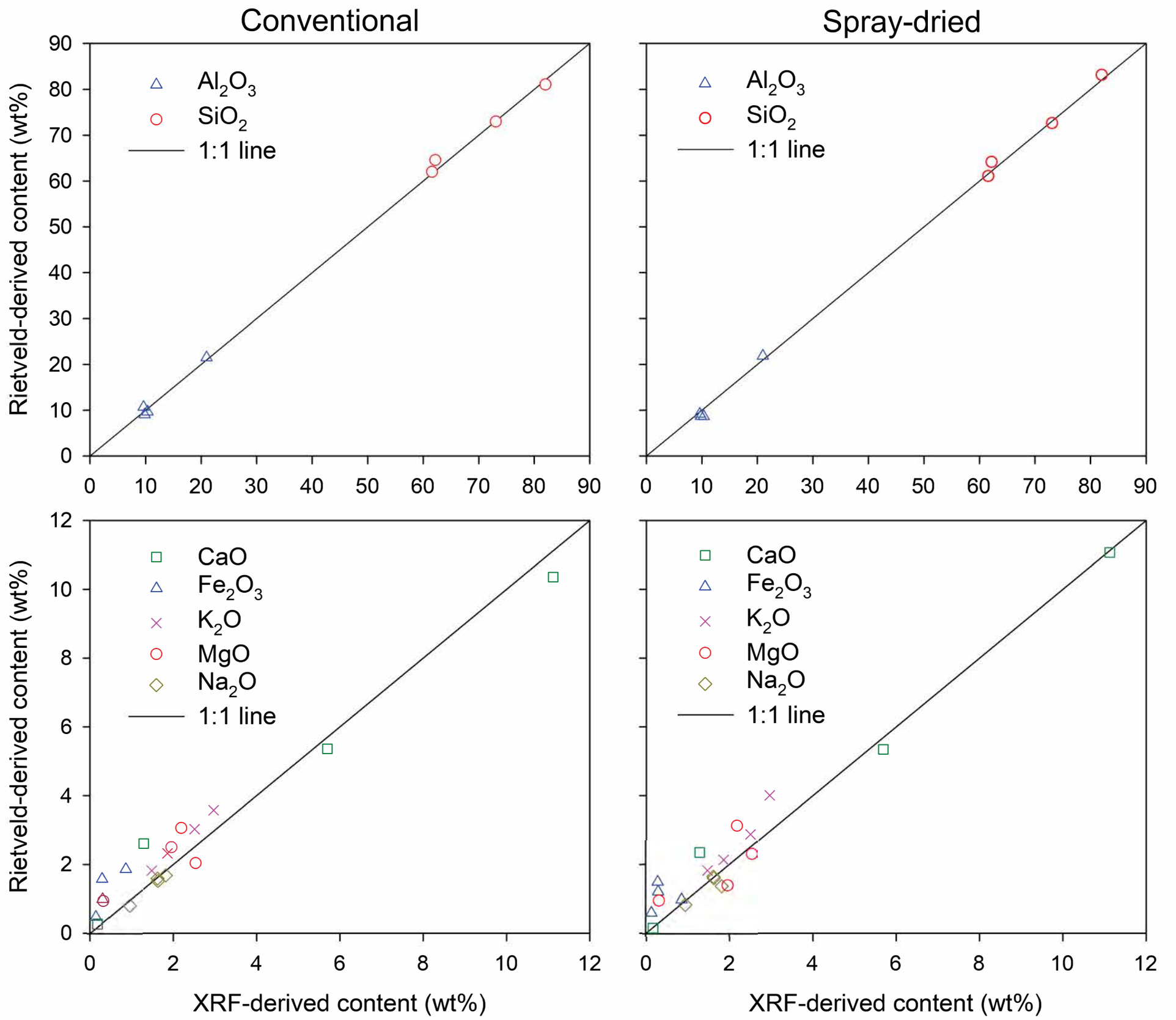
Conventional
Spray-dried
Rietveld-derived content (wt%)
XRF-derived content (wt%)
Al2O3
SiO2
CaO
Fe2O3
K2O
MgO
Na2O
1:1 line
0
10
20
30
40
50
60
70
80
90
2
4
6
8
12

Figure 14

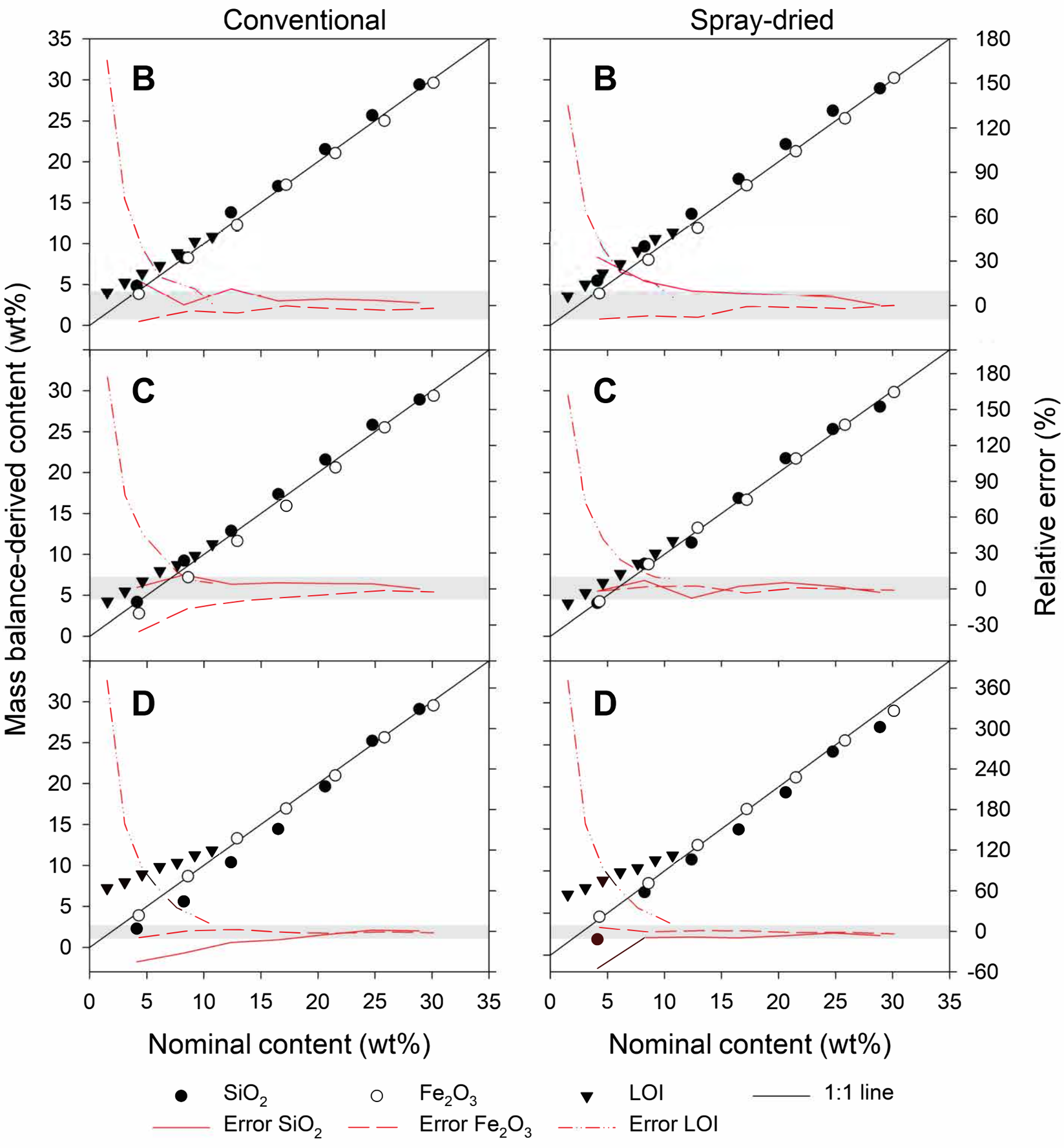
Conventional
Spray-dried
B
C
D
Mass balance-derived content (wt%)
Relative error (%)
Nominal content (wt%)
Nominal content (wt%)
SiO2
Fe2O3
LOI
1:1 line
Error SiO2
Error Fe2O3
Error LOI

Figure 15

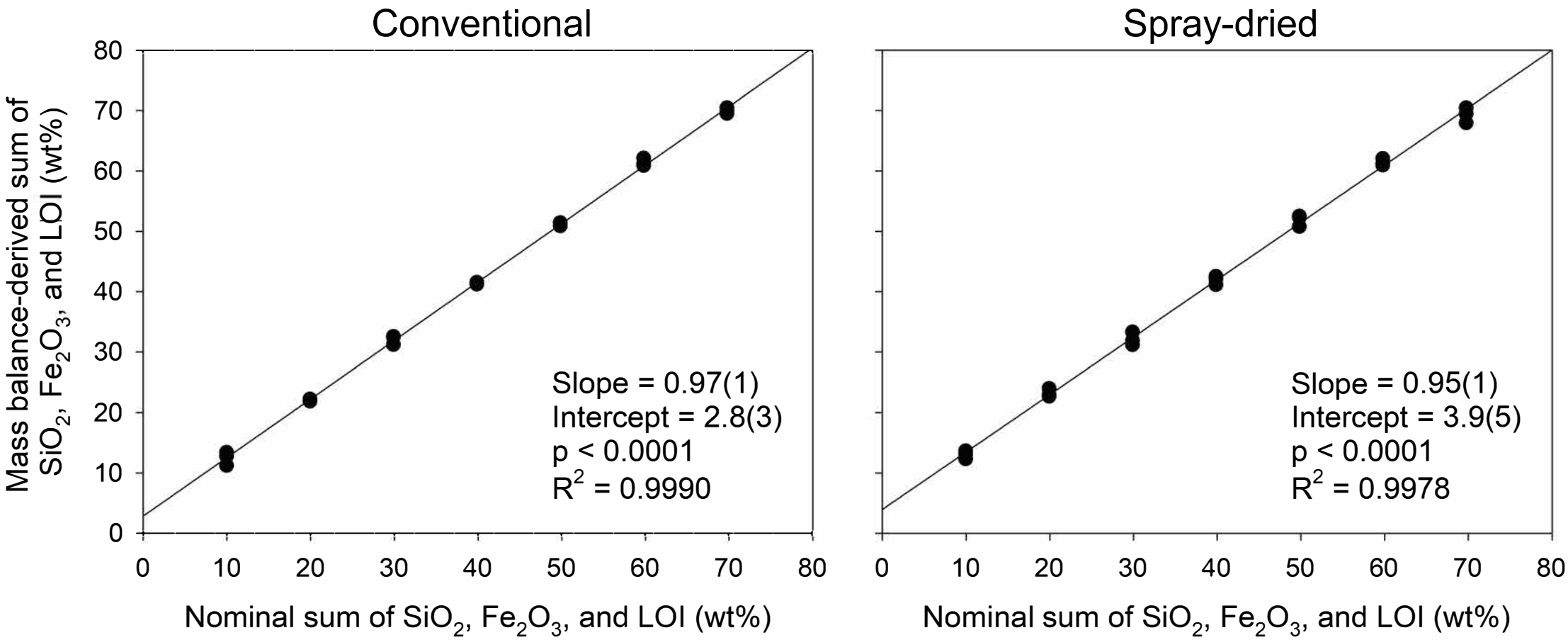
Conventional
Spray-dried
Mass balance-derived sum of SiO_2, Fe_2O_3, and LOI (wt%)
Nominal sum of SiO_2, Fe_2O_3, and LOI (wt%)
Slope = 0.97(1)
Intercept = 2.8(3)
p < 0.0001
R^2 = 0.9990
Slope = 0.95(1)
Intercept = 3.9(5)
p < 0.0001
R^2 = 0.9978
0
10
20
30
40
50
60
70
80